Original article

Radix Paeoniae Alba attenuates Radix Bupleuri-induced hepatotoxicity by modulating gut microbiota to alleviate the inhibition of saikosaponins on glutathione synthetase

Congcong Chen [a, b], Wenxia Gong [a, b], Junshen Tian [a, b], Xiaoxia Gao [a, b], Xuemei Qin [a, b], Guanhua Du [a, c], Yuzhi Zhou [a, b, *]

[a] Modern Research Center for Traditional Chinese Medicine, The Key Laboratory of Chemical Biology and Molecular Engineering of Ministry of Education, Shanxi University, Taiyuan, 030006, China
[b] Key Laboratory of Effective Substances Research and Utilization in TCM of Shanxi Province, Shanxi University, Taiyuan, 030006, China
[c] Institute of Materia Medica, Chinese Academy of Medical Sciences & Peking Union Medical College, Beijing, 100050, China

ARTICLE INFO

ABSTRACT

Radix Bupleuri (RB) is commonly used to treat depression, but it can also lead to hepatotoxicity after long-term use. In many anti-depression prescriptions, RB is often used in combination with Radix Paeoniae Alba (RPA) as an herb pair. However, whether RPA can alleviate RB-induced hepatotoxicity remain unclear. In this work, the results confirmed that RB had a dose-dependent antidepressant effect, but the optimal antidepressant dose caused hepatotoxicity. Notably, RPA effectively reversed RB-induced hepatotoxicity. Afterward, the mechanism of RB-induced hepatotoxicity was confirmed. The results showed that saiko-saponin A and saikosaponin D could inhibit GSH synthase (GSS) activity in the liver, and further cause liver injury through oxidative stress and nuclear factor kappa B (NF-κB)/NOD-like receptor thermal protein domain associated protein 3 (NLRP3) pathway. Furthermore, the mechanisms by which RPA attenuates RB-induced hepatotoxicity were investigated. The results demonstrated that RPA increased the abundance of intestinal bacteria with glycosidase activity, thereby promoting the conversion of saikosaponins to sai-kogenins in vivo. Different from saikosaponin A and saikosaponin D, which are directly combined with GSS as an inhibitor, their deglycosylation conversion products saikogenin F and saikogenin G exhibited no GSS binding activity. Based on this, RPA can alleviate the inhibitory effect of saikosaponins on GSS activity to reshape the liver redox balance and further reverse the RB-induced liver inflammatory response by the NF-κB/NLRP3 pathway. In conclusion, the present study suggests that promoting the conversion of saikosa-ponins by modulating gut microbiota to attenuate the inhibition of GSS is the potential mechanism by which RPA prevents RB-induced hepatotoxicity.

1. Introduction

Traditional Chinese medicines (TCMs) have been widely used to treat all kinds of diseases in Asia for thousands of years. Presently, based on the World Health Organization (WHO), approximately 80% of the global population relies on herbal medicines [1]. In recent years, with the widespread acceptance and recognition of TCM, an increasing number of clinical cases of hepatotoxicity induced by

herbs have been reported [2]. Especially in China, approximately 26.81% of clinical cases of hepatotoxicity are caused by herbal and dietary supplements [3]. Therefore, more attention should be given to the problem of hepatotoxicity caused by herbal medicines. Based on this, it is valuable to perform research on the combined detoxi-fication of herbal medicines based on the theory of TCM.

Radix Bupleuri (RB) is the dried root of the umbelliferous plant *Bupleurum chinense* DC, which was initially recorded in "Shen-nong's Classic of Material Medical" in 200 AD. RB is commonly used to treat depression by "soothing the liver and resolving melancholia". Modern pharmacological research has also confirmed that RB has antipyretic, sedative, anti-inflammatory, and antide-pressant effects [4]. With the steadily increasing use of RB, more attention has been focused on the safety of RB, such as the

---

hepatotoxicity of RB in clinical applications [5]. For example, in a review of adverse event reports of drug-induced liver injury from 2009 to 2014, RB-induced hepatotoxicity ranked top in the number of reported cases (11 of 57, 19.3%) [6]. Additionally, in traditional Chinese medicine (TCM) theory, the side effect of "robbing liver yin" of RB has been widely reported since the Ming Dynasties [7]. Furthermore, modern pharmacological studies have also confirmed that RB causes acute liver injury and hepatocyte apoptosis following overdose or long-term use [8]. Some components in RB, including saikosaponin A and saikosaponin D, have been reported to be hepatotoxic [9]. Altogether, although RB has antidepressant effects, the hepatotoxicity exhibited by RB limits its clinical application. In TCM theory, Radix Paeoniae Alba (RPA) has the effect of "nourishing blood and smoothing the liver", which can alleviate the "RB decreasing liver's yin essence" by mutual-detoxication compatibility rules. Furthermore, Radix Bupleuri-Radix Paeoniae Alba (RB-RPA) is also a common classic antidepressant herb pair and is considered the core drug pair in Xiaoyao powder, Sini powder, Chaihu Shugan powder, etc [10]. It achieves the effect of detoxification through the compatibility theory of "mutual detoxification". However, the mechanism by which RPA alleviates RB-induced hepatotoxicity remains unclear.

Glutathione (GSH) is a major endogenous antioxidant and redox signaling regulator. GSH protects organisms against oxidative damage by reducing H_2O_2 and scavenging reactive oxygen and nitrogen radicals [11]. Inhibition of GSH synthesis disrupts the hepatic redox balance system and induces liver oxidative injuries, which can further aggravate hepatotoxicity through tumor necrosis factor-α (TNF-α), nuclear factor kappa B (NF-κB), *c*-Jun *N*-terminal kinase (JNK), and mitochondrial apoptotic pathways [12]. Synthesis of GSH occurs through a two-step enzymatic reaction process. The first step is catalyzed by glutamate-cysteine ligase (GCL), and the second step is catalyzed by GSH synthase (GSS); among them, GCL is the rate-limiting enzyme for GSH synthesis. Although GSS is generally not considered important in regulating GSH synthesis, there is increasing evidence that GSS is important in GSH synthesis capacity in certain tissues or under stressful conditions [13,14]. For example, GSS activity and GSH levels were shown to be decreased after surgical trauma, while GCL activity was unchanged [15]. In rat hepatocytes, increased GSS expression further enhanced GSH synthesis [16,17]. In lung cancer cell lines and tumor-bearing nude mice, polydatin inhibits GSH synthesis capacity in tumors by inhibiting GSS activity, confirming that GSS is an effective antitumor target [18]. These results suggest that the regulation of GSS activity is also important for the overall GSH synthesis capacity. Moreover, GSS deficiency can lead to serious metabolic consequences, as accumulated γ-glutamylcysteine is converted to 5-oxoproline, which can cause severe metabolic acidosis and nervous system damage [17].

The gut microbiome can directly influence the drug action course by enzymatically transforming the drug's structure and altering its bioavailability, bioactivity, or toxicity—a phenomenon now known as pharmacomicrobiomics [19,20]. It has been reported in the literature that saikosaponins were mainly transformed into the corresponding saikogenins by intestinal microflora with glycosidase activity [21]. In addition, saikosaponins possess certain limitations, such as poor bioavailability and hepatotoxicity, which were significantly improved when converted to saikogenins [9,22,23]. Therefore, it is speculated that intestinal microflora has a certain influence on RB-induced hepatotoxicity, suggesting that the difference in gut microbiota composition may be the potential reason for different people to have different tolerance to RB-induced hepatotoxicity. In addition, some scholars speculated that saikosaponins were converted into saikogenins by intestinal microflora before absorption and then exerted pharmacological effects [24–26]. Our previous studies showed that the combined

use of RB and RPA could promote the conversion of saikosaponins to saikogenins in serum compared with RB alone [27]. Based on this, we speculate that RPA-suppressed RB-induced hepatotoxicity may be related to promoting the metabolic transformation of saikosaponins by regulating the intestinal flora.

2. Materials and methods

2.1. Materials and reagents

Traditional Chinese medicines RB and RPA were purchased from Shanxi Herintang Chinese Herbal Pieces Co., Ltd. (Taiyuan, China), and authenticated by Professor Xuemei Qin of the Shanxi University. Voucher specimens of the RB and RPA were deposited at Shanxi University, labeled as CCC-2021-0023 and CCC-2021-0024, respectively. Mass spectrometry-grade acetonitrile, methanol, and formic acid were purchased from Thermo Fisher Chemical Inc. (Waltham, MA, USA). Saikosaponin A, saikosaponin D, saikosaponin C, saikosaponin B_2, saikosaponin B_1, paeoniflorin, albiflorin, oxypaeoniflorin, and methyl gallate were purchased from Chengdu Ruifensi Biological Technology Co., Ltd. (Chengdu, China). Saikogenin A, saikogenin D, saikogenin E, saikogenin F, and saikogenin G were purchased from Shanghai Yuanye Biotechnology Co., Ltd. (Shanghai, China). L-glutamine, 5-oxoproline, γ-glutamylcysteine, reduced GSH, oxidized glutathione (GSSG), L-cysteine, L-glutamic acid, reserpine (IS1), and yohimbine (IS2) were purchased from Sigma Company (St. Louis, MO, USA). Anti-phospho-NF-κB (*p*-NF-κB), anti-NF-κB, anti-GSS, anti-NOD-like receptor thermal protein domain associated protein 3 (NLRP3), anti-caspase-1, anti-apoptosis-associated speck-like protein containing a CARD (ASC), anti-β-actin and horseradish peroxidase (HRP)-conjugated secondary antibodies were purchased from Beijing Boaosen Biotechnology Co., Ltd. (Beijing, China). Recombinant human GSS was purchased from ProSpec-Tany TechnoGene Ltd. (Ness-Ziona, Israel).

2.2. Preparation of herb extracts

According to the previous research method [10], for the extract of RB and RPA alone, 300 g RB or 300 g RPA were extracted twice with 70% ethanol (2400 mL), each time for 2 h. Then the extracts were concentrated and dried into lyophilized powder (the extraction rate of RB and RPA was 11.62% and 9.41%, respectively). For the extract of RB-RPA herb pairs, 300 g RB and 300 g RPA were mixed and soaked in 70% ethanol (4,800 mL), and then the RB-RPA herb pairs extracts were prepared according to the same procedure as above (the extraction rate of RB-RPA was 10.53%). Moreover, to ensure the quality of RB, RPA, and RB-RPA, the fingerprints were analyzed by ultra-high-performance liquid chromatography (UHPLC) [28]. For RB, the saikosaponin A, saikosaponin D, saikosaponin C, saikosaponin B_2, and saikosaponin B_1 were used as chemical markers for quality monitoring. For RPA, the albiflorin, paeoniflorin, oxypaeoniflorin, and methyl gallate were used as chemical markers for quality monitoring. The UHPLC chromatograms were shown in Fig. S1 and the content of the nine constituents in herb extracts was shown in Table S1. The results showed that compared with the single extract of RB, the co-decoction of RB and RPA did not affect the content of saikosaponins during the preparation of herbal extracts.

2.3. Animal

Healthy male Sprague-Dawley rats (180–220 g) were provided by Beijing Vital River Laboratory Animal Technology Co., Ltd. (Beijing, China), and the certificate number is SCXK (Jing) 2020–0034. All rats were acclimatized to their experimental environment for

one week before the experiments began, and allowed free access to food and water. The light cycle was 12/12 h dark/light. All animal experiments conformed to the NIH Guide for the Care and Use of Laboratory Animals, and the animal experiments were approved by the Experimental Animal Ethical Committee of Shanxi University (Approval number: SXULL2020028).

2.4. Drug administration and experimental design

After a week of acclimatization, all rats were randomly divided into 12 groups, 7 in each group: (1) Control group; (2) chronic unpredictable mild stress (CUMS) group; (3) RB1 group, oral administration of RB extract: 1.8 g-herb/kg; (4) RB2 group, oral administration of RB extract: 3.6 g-herb/kg; (5) RB3 group, oral administration of RB extract: 7.2 g-herb/kg; (6) RB4 group, oral administration of RB extract: 14.4 g-herb/kg; (7) RR1 group, oral administration of RB-RPA extract: 3.6 g-herb/kg (RB: RPA = 1:1); (8) RR2 group, oral administration of RB-RPA extract: 7.2 g-herb/kg (RB: RPA = 1:1); (9) RR3 group, oral administration of RB-RPA extract: 14.4 g-herb/kg (RB: RPA = 1:1); (10) RR4 group, oral administration of RB-RPA extract: 28.8 g-herb/kg (RB: RPA = 1:1); (11) RPA3 group, oral administration of RPA extract: 7.2 g-herb/kg; (12) RPA4 group, oral administration of RPA extract: 14.4 g-herb/kg. All rats were given the corresponding drugs twice a day for 49 days (in the morning and evening, 12 h intervals), and the gavage volume of each group was 10 mL/kg (rat body weight). The model of rats with depression was replicated by CUMS protocol as previously described [10], and the process was provided in Supplemental Method 1. Except for the Control group, the other groups were exposed to the CUMS procedure for 49 days. The experimental design is shown in Fig. S2.

2.5. Behavior test

The sucrose preference test (SPT), forced swim test (FST), and open-field test (OFT) were used to evaluate the antidepressant effects, as previously described [10]. The detailed processes of the SPT, OFT, and FST were provided in Supplemental Method 2. The tear secretion of Schirmer tear test (STT), water intake, sweat beads of the sweat test, rotation tolerance time on the rotating platform, stool moisture content, systolic blood pressure, and tongue features of rats were used to evaluate "liver yin deficiency" caused by RB. The detailed processes are provided in Supplemental Method 3.

2.6. Determination of oxidative stress index, inflammation index, liver injury index, β-D-fucosidase, and β-D-glucosidase

The activities of aspartate transaminase (AST) and alanine transaminase (ALT) in serum were determined by a commercial assay kit (Nanjing Jiancheng Bioengineering Institute, Nanjing, China). Liver tissue homogenates were prepared to measure superoxide dismutase (SOD) and glutathione peroxidase (GSH-Px) activities, and malondialdehyde (MDA), GSH, and GSSG levels by the commercial assay kits (Nanjing Jiancheng Bioengineering Institute, Nanjing, China). The activities of GSS were determined by a commercial assay kit (Changzhou Beiyuanxin Biotechnology Co., Ltd., Changzhou, China) by the manufacturer's instructions. Briefly, the liver tissue samples were homogenized for 2 min in ice-cold physiological saline (1:9, m/V), and centrifuged at 3,000 rpm for 10 min at 4 °C. The protein levels in the liver tissue homogenates were measured by a bicinchoninic acid (BCA) protein kit, and the absorbance was measured using a microplate spectrophotometer (Infinite M200 PRO, TECAN Inc. Männedorf, Switzerland).

The levels of interleukin-1β (IL-1β), interleukin-6 (IL-6), tumor necrosis factor-α (TNF-α), and cytokeratin 18 (CK-18) in liver tissue homogenates, and β-D-fucosidase, and β-D-glucosidase in colon contents samples were measured by enzyme-linked immunosorbent assay (ELISA) kits, and all experimental procedures were carried out by the instructions provided by the manufacturers (AndyGene Biotechnology Co., Ltd., Beijing, China).

2.7. Histopathology assessments

The liver tissues were fixed in a 10% paraformaldehyde solution. And liver tissues were sectioned at 5–6 μm in paraffin wax, and then stained with hematoxylin-eosin (H&E). The histopathology assessment images were acquired by a light microscope (Olympus, Tokyo, Japan).

2.8. Western blot

The liver tissue samples were homogenized in radioimmunoprecipitation assay (RIPA) lysis buffer containing 1% phenylmethanesulfonyl fluoride (PMSF) and incubated on ice for 1 h. The homogenates were centrifuged at 13,000 rpm for 15 min at 4 °C, and the supernatants were collected. The protein levels were determined by a bicinchoninic acid (BCA) protein kit. The protein was separated by using 10% sodium dodecyl-sulfate polyacrylamide gel electrophoresis (SDS-PAGE) (Epizyme Biomedical Technology Co., Ltd, Shanghai, China) and transferred to polyvinylidene fluoride (PVDF) membranes (EMD Millipore, Billerica, MA, USA). After blocked with Tris-buffered saline containing 5% (m/V) non-fat milk for 2 h and incubated with the appropriate primary antibodies at 4 °C overnight: GSS (1:1000), p-NF-κB p65 (1:1000), NF-κB p65 (1:1000), NLRP3 (1:1000), caspase-1 (1:1000), ASC (1:1000), and β-actin (1:1000). The membranes were washed three times by 5% skim milk and incubated with HRP-conjugated antibodies (1:5000) at room temperature for 2 h, and the membranes were scanned using the fluorescent scanner.

2.9. Molecular docking

The crystal structures of the GSS were obtained from the Protein Data Bank (PDB) database (https://www.rcsb.org/). The enzyme structures were pre-processed in Autodock Tools 4.2.6 to add hydrogen and calculate the Gasteiger charges. The structures of saikosaponin A, saikosaponin D, saikogenin F, saikogenin G, and γ-glutamylcysteine were obtained from the ZINC database (https://zinc.docking.org/). The semi-flexible docking mode of the docking ligand (CDOCKER) program in the Discovery Studio 2016 software was used to perform molecular docking analysis. The binding site was selected using the grid generation procedure. The CDOCKER was selected for molecular docking analysis.

2.10. Isothermal titration calorimetry (ITC) assay

A Microcal ITC 200 calorimeter (Malvern Panalytical, Marvin, UK) was used to measure the kinetic constant (K_d) values of GSS when binding with saikosaponin A, saikosaponin D, saikogenin F, and saikogenin G. The solutions of the proteins and the ligand both contain 1% glycerol, 100 μM Tris−HCl (pH 8.0), and 1% dimethyl sulfoxide (DMSO). The titration was started with a 100 μM small-molecule infusion into 10 μM GSS protein solution and followed by the default ITC procedure. The raw data were fitted using a single-site binding model to calculate the K_d value.

2.11. Atomic force microscopy (AFM) imaging technology

GSS protein was dissolved in 100 μM Tris−HCl (pH 8.0) and 1% DMSO, diluted to 0.1 μM, with 0.3 μM of saikosaponin A,

saikosaponin D, saikogenin F, and saikogenin G solution, respectively. The protein solution was mixed with the small molecule ligand solution at 1:1 and 30 min was incubated at 37 °C. Then, the protein solution and the incubation solution were crystallized for 30 min at 37 °C on silicon wafers. After balance, MultiMode 8-HR AFM (Bruker, Berlin, Germany) was used to scan protein crystals and protein-small molecule complex crystals with parameters of 0.98 Hz, 20 μm × 20 μm in tap mode. The morphology, distribution, and aggregation of protein crystals on each silicon wafer were observed. NanoScope Analysis 1.8 was used to process the captured images.

2.12. In vitro GSS inhibitory activity assay

The inhibitory activities of GSS were detected by a commercial assay kit (Changzhou Beiyuanxin Biotechnology Co., Ltd.). Briefly, saikosaponin A, saikosaponin D, saikogenin F, and saikogenin G were treated in the enzyme cocktail prepared from rat liver homogenates or in recombinant human glutathione synthetase. After pre-incubation of the enzyme mixture for 60 min at 37 °C, the inhibitory activities of GSS were determined according to the manufacturer's instructions. The detailed sample preparation protocol can be found in Supplemental Method 4.

2.13. Collection and preparation of serum, liver tissues, and colon contents samples for ultra high performance liquid chromatography coupled with mass spectrometry (UHPLC-MS/MS) analysis and targeted quantitative analysis

The collection and preparation of serum, liver tissues, and colon contents samples were conducted as described in previous reports [29,30], and the detailed processes are provided in Supplemental Method 5.

2.14. The method for pharmacochemistry analysis and metabolomics analysis of liver tissues samples

Using Thermo-Fisher Dionex UltiMate 3000 UHPLC-Q Exactive Orbitrap-mass spectrometer (UHPLC-Q-Orbitrap/MS) and Xcalibur workstation (Thermo Fisher, Waltham, MA, USA) were used to acquire raw data. The complete details of the UHPLC-Q-Orbitrap/MS method for pharmacochemistry analysis and metabolomics analysis are provided in Supplemental Method 6.

2.15. UHPLC-MS/MS data processing for pharmacochemistry analysis of liver tissues samples

The different chemical compositions in liver tissue samples between the RB4 group and RR4 group were analyzed by integrating background subtraction and multivariate statistical analysis techniques, as previously described [27]. The differential chemical compositions were identified by the retention times, accurate molecular weight, and product ion mass spectrometry data (MS/MS) with the authentic reference standard, database, and Compound Discoverer 3.0 workstation. The detailed processes of the background subtraction algorithm and the multivariate statistical analysis are provided in Supplemental Method 7 and Supplemental Method 8, respectively.

2.16. UHPLC-MS/MS data processing for liver metabolomics analysis

The metabolomics raw data were imported to Compound Discoverer 3.0 (Thermo Fisher) to obtain the matched peak data, and the peak area data was normalized in Microsoft Excel 2020. The detailed processes of the metabolomics data processing parameters in Compound Discoverer 3.0 software and Microsoft Excel 2020 are provided in Supplemental Method 9. Furthermore, the obtained endogenous metabolites data were further imported into soft independent modeling of class analogy (SIMCA) 16.0 (Umetrics, Stockholm, Sweden) for multivariate statistical analysis, and the significant difference endogenous metabolites were screened according to the variable importance for the projection (VIP) values (VIP >1) and t-test ($P < 0.05$). Metabolites were identified according to m/z values, retention time, molecular formula, and MS/MS fragments in the online databases including Human Metabolome Database (http://www.hmdb.ca), Massbank (http://www.massbank.jp), Kyoto Encyclopedia of Genes and Genomes (http://www.kegg.jp), PubChem (https://pubchem.ncbi.nlm.nih.gov/), Lipid Maps (http://www. lipidmaps.org) and Metlin (http://metlin.scripps.edu).

2.17. Quantitative analysis of the saikosaponins, saikogenins, and glutathione metabolites

The quantitative analysis of saikosaponin A, saikosaponin D, saikosaponin C, saikosaponin B_2, saikosaponin B_1, saikogenin A, saikogenin D, saikogenin F, saikogenin E, and saikogenin G in liver tissues samples were performed on a Thermo-Fisher Dionex UltiMate 3000 UHPLC-Q Exactive Orbitrap-MS, and quantitative data were acquired using parallel reaction monitoring (PRM) mode. The quantitative product ion and collision energy (CE) for the 10 reference standards were optimized using the MS Tune software (Thermo Fisher) and are shown in Table S2. Data were processed using the Xcalibur workstation. The liquid chromatography, mass spectrometry methods, and method validation are provided in Supplemental Method 10.

The quantitative analysis of saikosaponin A, saikosaponin D, saikosaponin C, saikosaponin B_2, saikosaponin B_1, saikogenin A, saikogenin D, saikogenin F, saikogenin E, and saikogenin G in colon contents samples, and ʟ-glutamine, 5-oxoproline, γ-glutamylcysteine, GSH, GSSG, ʟ-cysteine, and ʟ-glutamic acid in liver tissues samples was performed on an Agilent 1290 series UHPLC system (Agilent Technologies, Santa Clara, CA, USA) combined with an AB SCIEX 3200 Q-TRAP (AB SCIEX, Framingham, MA, USA), using multiple reaction monitoring (MRM) modes to acquire the quantitative data [31]. The compound-dependent parameters, including MRM ion pairs, CE, and declustering potential (DP) are listed in Tables S3 and S4. The liquid chromatography, mass spectrometry methods, and method validation are provided in Supplemental Method 11.

2.18. 16S rRNA third-generation full-length sequencing of gut microbiota

Colon contents samples were collected from the RB4 group ($n = 7$), RPA4 group ($n = 7$), and RR4 group ($n = 7$). Total DNA was extracted from colonic contents using a QIAamp-DNA Stool Mini Kit (Qiagen, Hilden, Germany). Sequencing of the polymerase chain reaction (PCR) amplification products was performed on an Illumina Miseq platform at Majorbio Bio-Pharm Technology Co., Ltd. (Shanghai, China). The full-length 16S rRNA sequence was amplified using the universal PCR primers 27F (5′-AGAGTTT-GATCMTGGCTCAG-3′) and 1492R (5′-ACCTTGTTACGACTT-3′). The generated optimization circular consensus sequencing (CCS) was clustered at the level of 100% similarity, and its species classification was obtained based on the sequence composition of the absolute Sequence Variants (ASV). The National Center for Biotechnology Information (NCBI) database (ftp://ftp.ncbi.nih.gov/blast/db/) was used to analyze species annotation and the
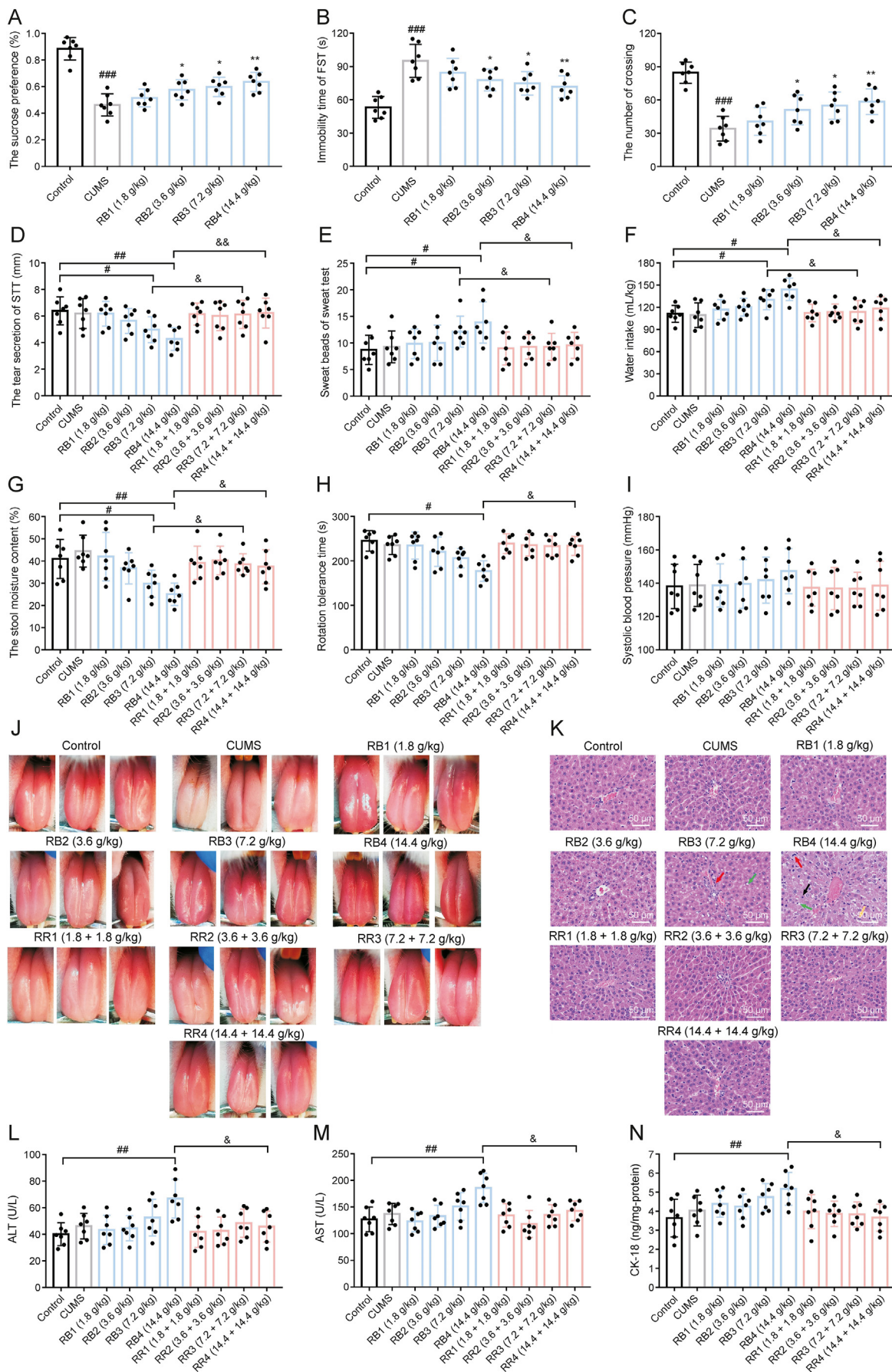
diversity of gut microbiota. Analyses for rarefaction curves and calculation of richness estimators and diversity indices were performed using the Quantitative Insights Into Microbial Ecology 2 (QIIME2) program.

2.19. Statistical analyses

All values are presented as the mean ± standard deviation (SD). Data were statistically analyzed using GraphPad Prism 8 software (San Diego, CA, USA). Statistical analyses from two groups were compared using a two-tailed Student's *t*-test, and data from more groups were compared with a one-way analysis of variance (ANOVA) followed by Dunnett's post hoc test. $P < 0.05$ was considered significant.

3. Results and discussion

3.1. RB has a dose-dependent antidepressant effect, but the optimal antidepressant dose of RB causes "liver yin deficiency"-like behavior and hepatotoxicity

The antidepressant effects of RB were evaluated by SPT, FST, and OFT. After 49 days of CUMS treatment, the CUMS group rats showed obvious depression-like behaviors (Figs. 1A–C, SPT, $P < 0.001$; FST, $P < 0.001$; OFT, $P < 0.001$ compared with the Control group, respectively), which revealed that the CUMS model was replicated successfully. After 49 days of RB administration, RB (1.8–14.4 g-herb/kg) improved the behavioral indicators that reflected the depression status in a concentration-dependent manner (Figs. 1A–C), and among them, 14.4 g-herb/kg RB had the best antidepressant effect (SPT, $P < 0.01$; FST, $P < 0.01$; OFT, $P < 0.01$ compared with the CUMS group). Additionally, the "liver yin deficiency" side effects of RB were assessed by the tear secretion of STT, water intake, sweat beads of the sweat test, rotation tolerance time on the rotating platform, stool moisture content, systolic blood pressure, and tongue features of rats. And the hepatotoxicity of RB was assessed by AST, ALT, CK-18, and liver histopathological examination. The results showed that 7.2 and 14.4 g-herb/kg RB caused the side effects of "liver yin deficiency"-like behavior, including dry eyes (Fig. 1D), diaphoretic (excessive sweating, Fig. 1E), xerostomia (Fig. 1F), dry stools (Fig. 1G), dizziness (Fig. 1H), and reddish tongue (Fig. 1J). Moreover, the activity of ALT and AST in serum and the levels of CK-18 in liver tissue are commonly used indices to reflect drug-induced hepatotoxicity [32,33]. Histologic assessments demonstrated that liver injury occurred after treatment with 14.4 g-herb/kg RB (Fig. 1K), including nuclear pyknosis (dark arrows), inflammatory cell infiltration (red arrows), hepatocyte watery degeneration (yellow arrows), and hepatocyte steatosis (green arrows). From Fig. 1L–N, 14.4 g-herb/kg RB significantly increased the serum ALT and AST activity and the liver tissue CK-18 levels compared with the control group. These data suggest that 14.4 g-herb/kg RB has the potential to cause hepatotoxicity. These results indicated that although 14.4 g-herb/kg RB has the best antidepressant effect, it can also cause toxic side effects.

3.2. RPA reverses the "liver yin deficiency"-like behavior and hepatotoxicity induced by RB in CUMS depression model rats

As shown in Figs. 1D–J, the combined use of RPA and RB (RR3 group and RR4 group) reversed the "liver yin deficiency"-like behavior induced by 7.2 and 14.4 g-herb/kg RB. Meanwhile, the combined use of RPA and RB (RR4 group) significantly decreased the elevated serum ALT and AST activities and liver tissue CK-18 levels induced by 14.4 g-herb/kg RB (Figs. 1L–N). Furthermore, liver histological assessments also demonstrated the protective effect of RPA against RB-induced liver injury, including reduced nuclear pyknosis and decreased inflammatory cell infiltration (Fig. 1K). These results indicated that the combined use of RPA and RB reverses the "liver yin deficiency"-like behavior and hepatotoxicity induced by RB. Interestingly, the antidepressant effect of the combination of RB and RPA was also significantly better than that of RB or RPA alone in the SPT, OFT, and FST (Fig. S3).

3.3. Metabolomic techniques and biological network analysis identifies GSS as a potential target of RPA to reverse RB-induced hepatotoxicity

The principal component analysis (PCA) score plots built with liver metabolomics showed a clear separation between RB4 (RB-induced hepatotoxic dose group) and Control, CUMS, RB2 (RB nontoxic side effect dose group), and RR4 (attenuated group after combined use of RB and RPA), and all the quality control (QC) samples were closely correlated (Figs. 2A and B). In this study, the differential metabolites overlapped by the RB4 group and other groups were considered as the key metabolites only related to hepatotoxicity. The differential metabolites between RB4 and Control, CUMS, RB2, and RR4 were screened according to the S-plot (<-0.58 or >0.58), VIP value (>1.0), and *t*-test ($P < 0.05$) (Fig. S4). As shown in Figs. 2C and D, a total of 37, 33, 26, and 43 differential metabolites were identified between RB4 and Control, RB4 and RB2, RB4 and RR4, and RB4 and CUMS, respectively (Tables S5–S8). Among them, a total of 10 overlapping differential metabolites (ornithine, L-glutamine, 5-oxoproline, α-ketoglutaric acid, γ-glutamylcysteine, xanthosine, *cis*-aconitic acid, oxalosuccinate, GSH, and GSSG) were shared between RB4 and Control, RB4 and RB2, RB4 and RR4, and RB4 and CUMS (Fig. 2D). The results of the receiver operating characteristic (ROC) curve analysis demonstrated that the areas under the curve of the 10 differential metabolites were greater than 0.8 (Fig. S5). Therefore, these 10 differential metabolites could be defined as potential biomarkers for RB-induced hepatotoxicity. Furthermore, the 10 key metabolites were imported into MetaboAnalyst for pathway analysis. The results showed that glutathione metabolism had the greatest pathway impact in both the metabolic pathway analysis and the pathway enrichment analysis (Fig. 2E). Next, an interaction network analysis of the metabolite-enzyme network was constructed by the "pathway-based" mode in Metscape (embedded in Cytoscape v.3.7.0). The metabolite-enzyme network results showed that GSS was the enzyme connected between two dysregulated metabolites (Fig. 2F). Among them, the GSS enzyme substrate (γ-glutamylcysteine) was significantly increased, and the enzyme product

Fig. 1. The combined use of RPA and RB (RR group) reversed RB-induced "liver Yin deficiency" and hepatotoxicity in CUMS depression model rats. (A) Sucrose preference. (B) Immobility time in the FST. (C) The number of crossings in the OFT. (D) The tear secretion of the STT. (E) Sweat beads of the sweat test. (F) Water intake. (G) Stool moisture content. (H) Rotation tolerance time on the rotating platform. (I) Systolic blood pressure. (J) The tongue features of rats. (K) Liver histological examination (dark arrows: nuclear pyknosis; red arrows: inflammatory cell infiltration; yellow arrows: hepatocyte watery degeneration; green arrows: hepatocyte steatosis). (L) Serum ALT levels. (M) Serum AST level. (N) CK-18 in liver tissue. CUMS: chronic unpredictable mild stress; FST: forced swim test; OFT: open-field test; STT: schirmer tear test; ALT: alanine transaminase; AST: aspartate transaminase; CK-18: cytokeratin 18; RPA: Radix Paeoniae Alba; RB: Radix Bupleuri; RR: Radix Bupleuri-Radix Paeoniae Alba herb pair. All data are expressed as the mean ± standard deviation (SD) ($n = 7$). P values were calculated using two-tailed Student's *t*-test for paired comparisons or one-way analysis of variance (ANOVA) for multiple comparisons. $^{\#}P < 0.05$, $^{\#\#}P < 0.01$ compared with the control group; $^{*}P < 0.05$, $^{**}P < 0.01$ compared with the CUMS group; and $^{\&}P < 0.05$, $^{\&\&}P < 0.01$ compared with the RB group.
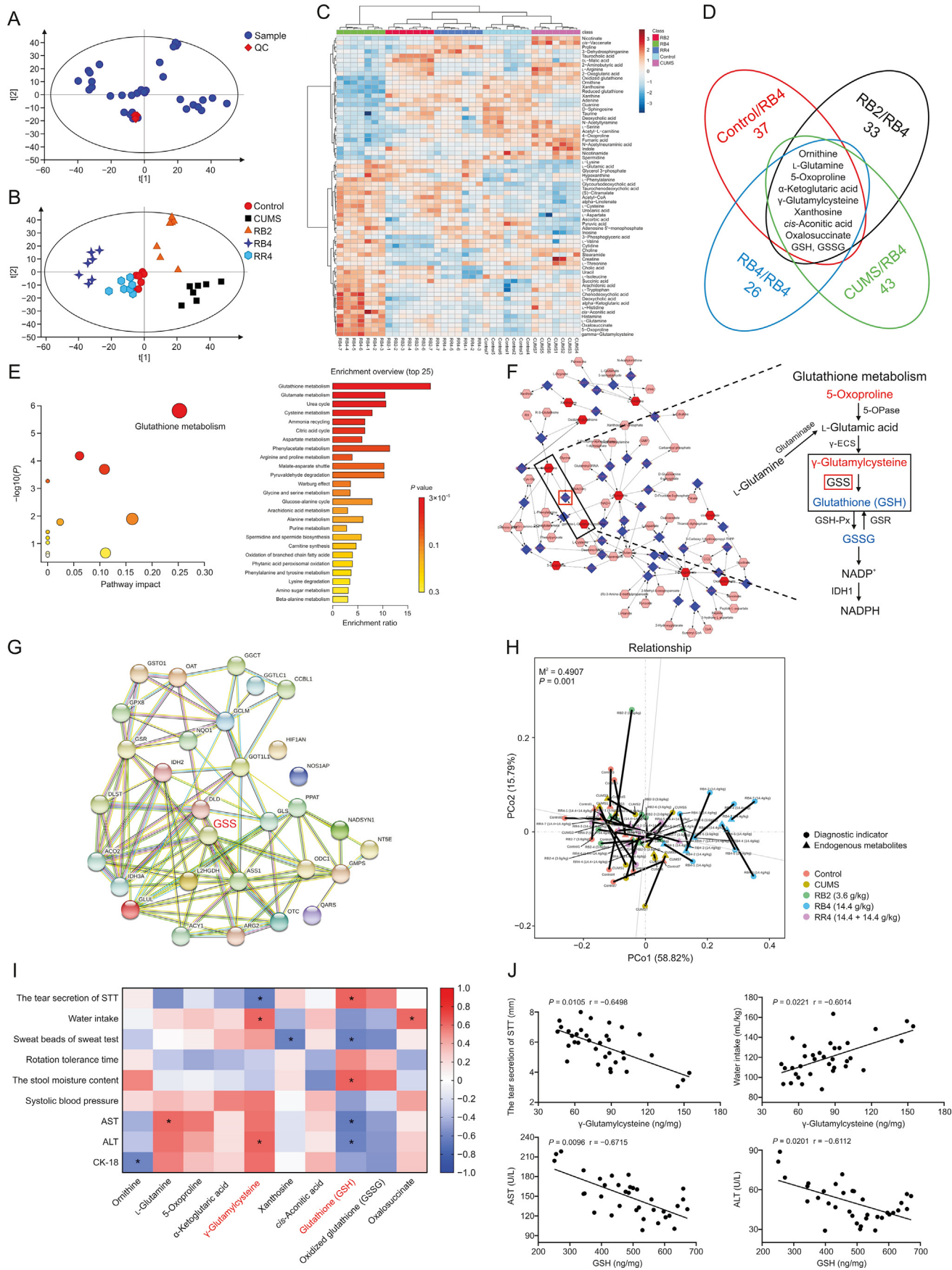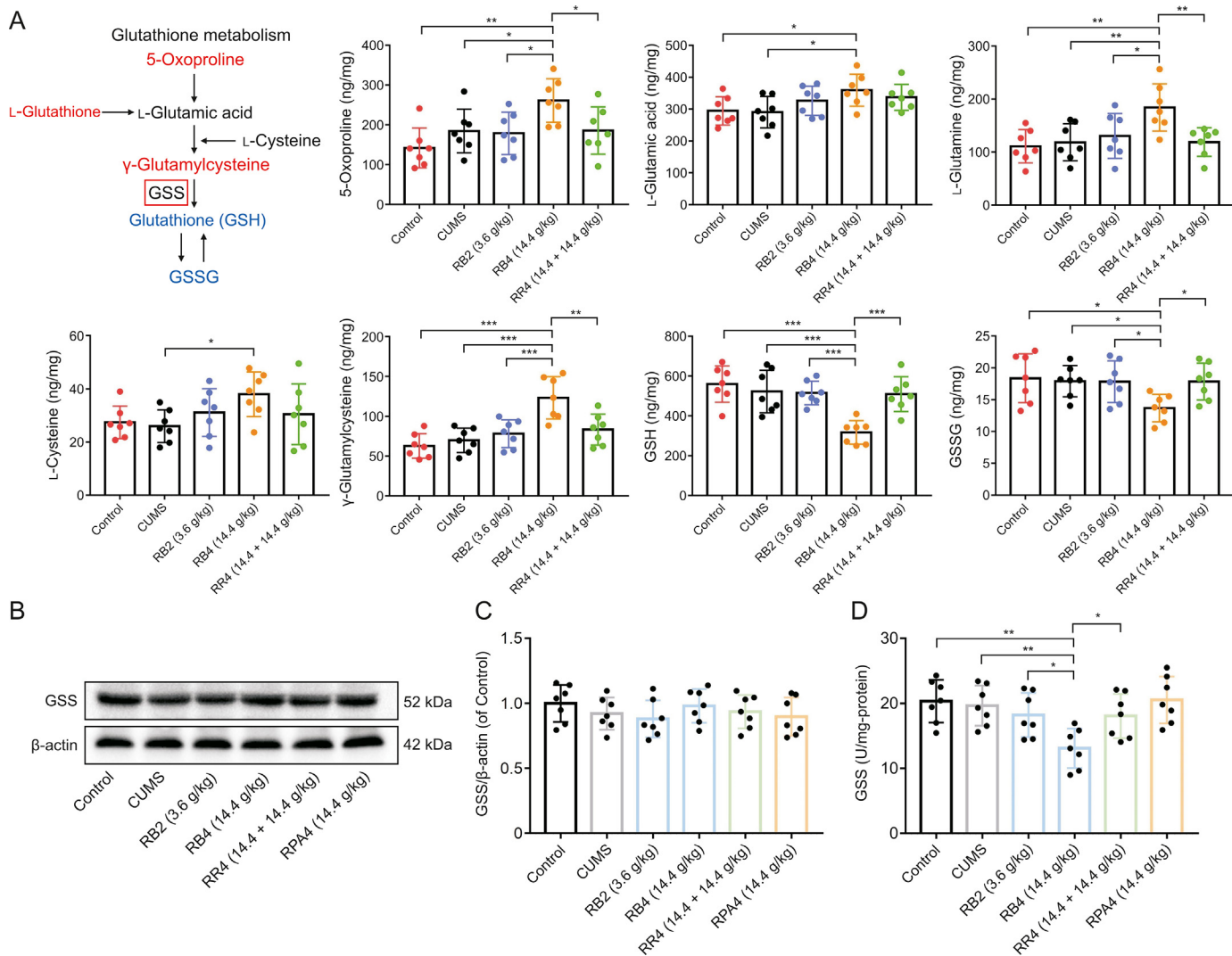
Fig. 3. Targeted quantitative analysis of the glutathione metabolism pathway and determination of GSS protein expression and activity. (A) Concentration (ng/mg) of 10 metabolites related to the glutathione metabolism pathway in the rat liver. The metabolites marked as red, blue, or black represent those that were upregulated, downregulated, or unchanged after RB4 exposure, respectively. (B) Determination of GSS protein expression levels. (C) Quantitative densitometric analysis of GSS protein. (D) Determination of GSS activity. GSH: glutathione; GSSG: oxidized glutathione; GSS: glutathione synthetase; RB: Radix Bupleuri; RPA: Radix Paeoniae Alba; RR: Radix Bupleuri-Radix Paeoniae Alba herb pair. All data are expressed as the mean ± standard deviation (SD) ($n = 7$). P values were calculated using one-way analysis of variance (ANOVA) for multiple comparisons. $^{*}P < 0.05$, $^{**}P < 0.01$, and $^{***}P < 0.001$ compared with the RB4 group.

(GSH) was significantly decreased in the RB4 group compared with the Control, CUMS, RB2, and RR4 groups. Moreover, protein-protein interaction (PPI) analysis results also demonstrated that GSS plays an important role in the disturbance of RB-induced hepatotoxicity metabolic network (Fig. 2G). Furthermore, Procrustes analysis results showed that there was a good correlation between the

hepatotoxicity index and the 10 key metabolites (Fig. 2H, $M^2 = 0.4907$, $P = 0.001$). The Pearson correlation analysis further confirmed the correlation between RB-induced toxic side effects index and 10 key metabolites, and the results showed that there was a significant correlation between the substrates and products of GSS and RB-induced toxic side effects index (Figs. 2I and S6). For

Fig. 2. Metabolomic and biological network analyses identified GSS as a potential target of RPA to reverse RB-induced hepatotoxicity. (A) Principal component analysis (PCA) score plots from the analysis sample and QC to investigate instrument stability for large-scale sample analysis ($n = 7$). (B) PCA score plots from the control group, CUMS group, RB2 group, RB4 group, and RR4 group ($n = 7$). (C) Hierarchical clustering analysis heatmap of differential metabolites. Maroon or navy blue represents that the levels of differential metabolites were higher or lower compared to the average level, respectively. Rows indicate the differential metabolites, and columns represent the analysis samples of rats ($n = 7$). (D) Venn diagram of significant differential metabolites between RB4 and Control, RB4 and RB2, RB4 and RR4, and RB4 and CUMS. The 10 overlapping differential metabolites are listed. (E) Met-PA pathway analysis and enrichment pathway analysis of 10 key differential metabolites. (F) The metabolite-enzyme network was constructed by the "pathway-based" mode in Metascape (embedded in Cytoscape v.3.7.0). The nodes marked in red, pink, and blue represent the input differential metabolites, other associated metabolites, and linked differential metabolite-related enzymes, respectively. (G) Protein-protein interaction (PPI) analysis of the linked differential metabolite-related enzymes. (H) Procrustes analysis between the hepatotoxicity index and the 10 key metabolites. (I) Heatmap of Pearson correlation analysis between 10 key metabolites and behavior indicators related to "liver yin deficiency" and biochemical indicators related to liver injury. Red indicates that r was a positive value, and blue indicates that r was a negative value. The darker the color, the larger the |r|. * means $P < 0.05$ and $|r| > 0.6$. (J) Scatter plot of the correlation analysis. CUMS: chronic unpredictable mild stress; QC: quality control; GSS: glutathione synthetase; PCo: principal coordinate; STT: Schirmer tear test; ALT: alanine transaminase; AST: aspartate transaminase; CK-18: cytokeratin 18; RB: Radix Bupleuri; RR: Radix Bupleuri-Radix Paeoniae Alba herb pair.
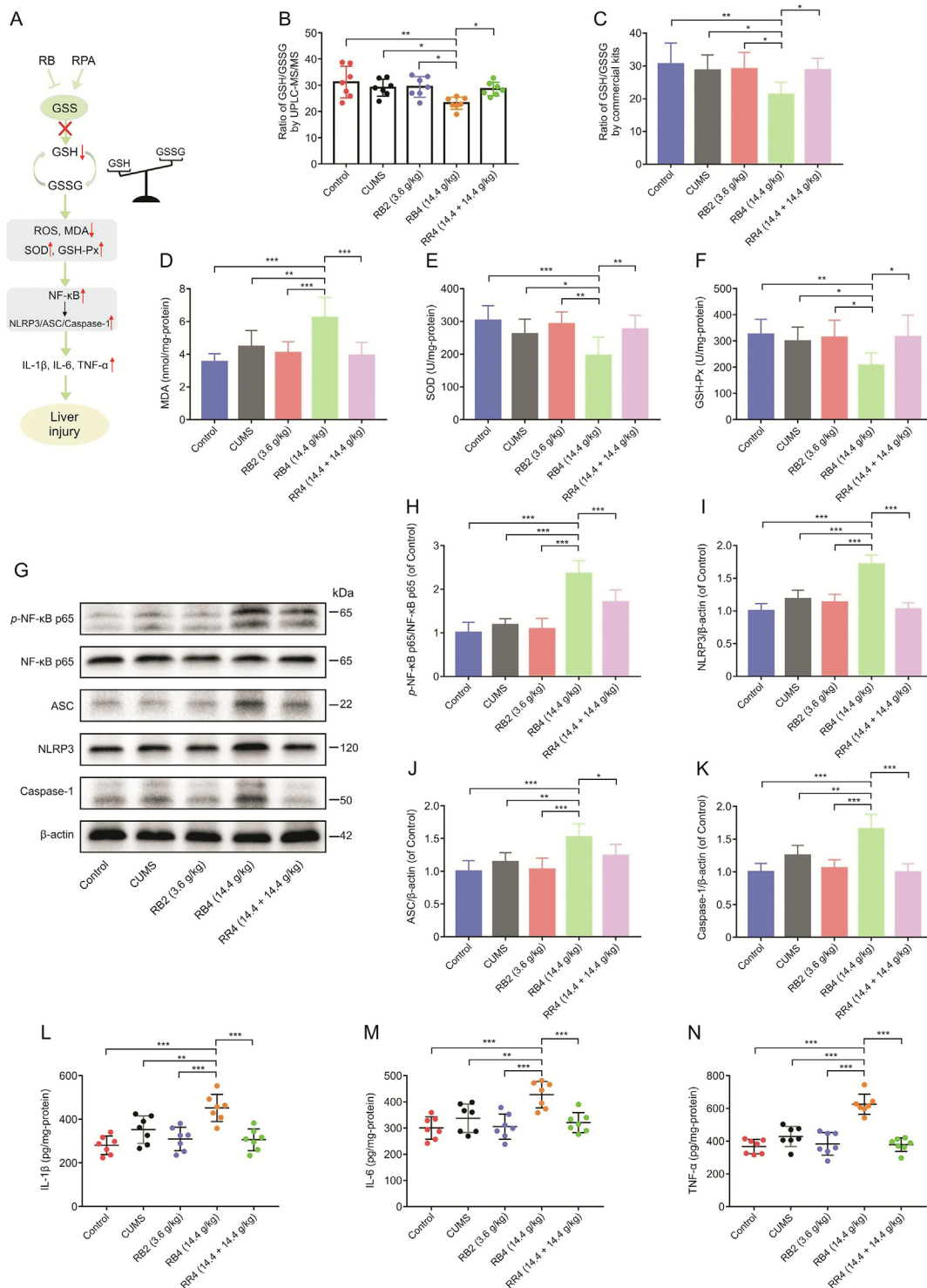
Fig. 4. The combined use of RPA and RB (RR group) suppresses RB-induced hepatotoxicity via oxidative stress and the NF-κB/NLRP3 pathway. (A) Schematic illustration of GSS inhibition leading to liver injury through activated oxidative stress and NF-κB pathways. (B) The ratio of GSH/GSSG was determined by UPLC–MS/MS quantitative analysis. (C) The ratio of GSH/GSSG was determined by enzyme-linked immunosorbent assay (ELISA) kits. (D) MDA in liver tissue. (E) SOD in liver tissue. (F) GSH-Px in liver tissue. (G) Protein levels of phosphorylated NF-κB p65, total NF-κB p65, NLRP3, caspase-1, and ASC were measured by western blotting. (H) Quantitative densitometric analysis of the ratio of phosphorylated NF-κB p65 to total NF-κB p65 (p-NF-κB p65/NF-κB p65). (I) Quantitative densitometric analysis of NLRP3 protein. (J) Quantitative densitometric analysis of ASC protein. (K) Quantitative densitometric analysis of caspase-1 protein. (L) IL-1β in liver tissue. (M) IL-6 in liver tissue. (N) TNF-α in liver tissue. GSH: glutathione; GSSG: oxidized glutathione; GSS: glutathione synthetase; MDA: malondialdehyde; SOD: superoxide dismutase; GSH-Px: glutathione peroxidase; ROS: reactive oxygen species; NF-κB: nuclear factor kappa B; NLRP3: NOD-like receptor thermal protein domain associated protein 3; ASC: apoptosis-associated speck-like protein containing a CARD; IL-1β: interleukin-1β; IL-6: interleukin-6; TNF-α: tumor necrosis factor-α; RB: Radix Bupleuri; RPA: Radix Paeoniae Alba; RR: Radix Bupleuri-Radix Paeoniae Alba herb pair. All data are expressed as the mean ± standard deviation (SD) ($n = 7$). P values were calculated using one-way analysis of variance (ANOVA) for multiple comparisons. $^*P < 0.05$, $^{**}P < 0.01$, and $^{***}P < 0.001$ compared with the RB4 group.
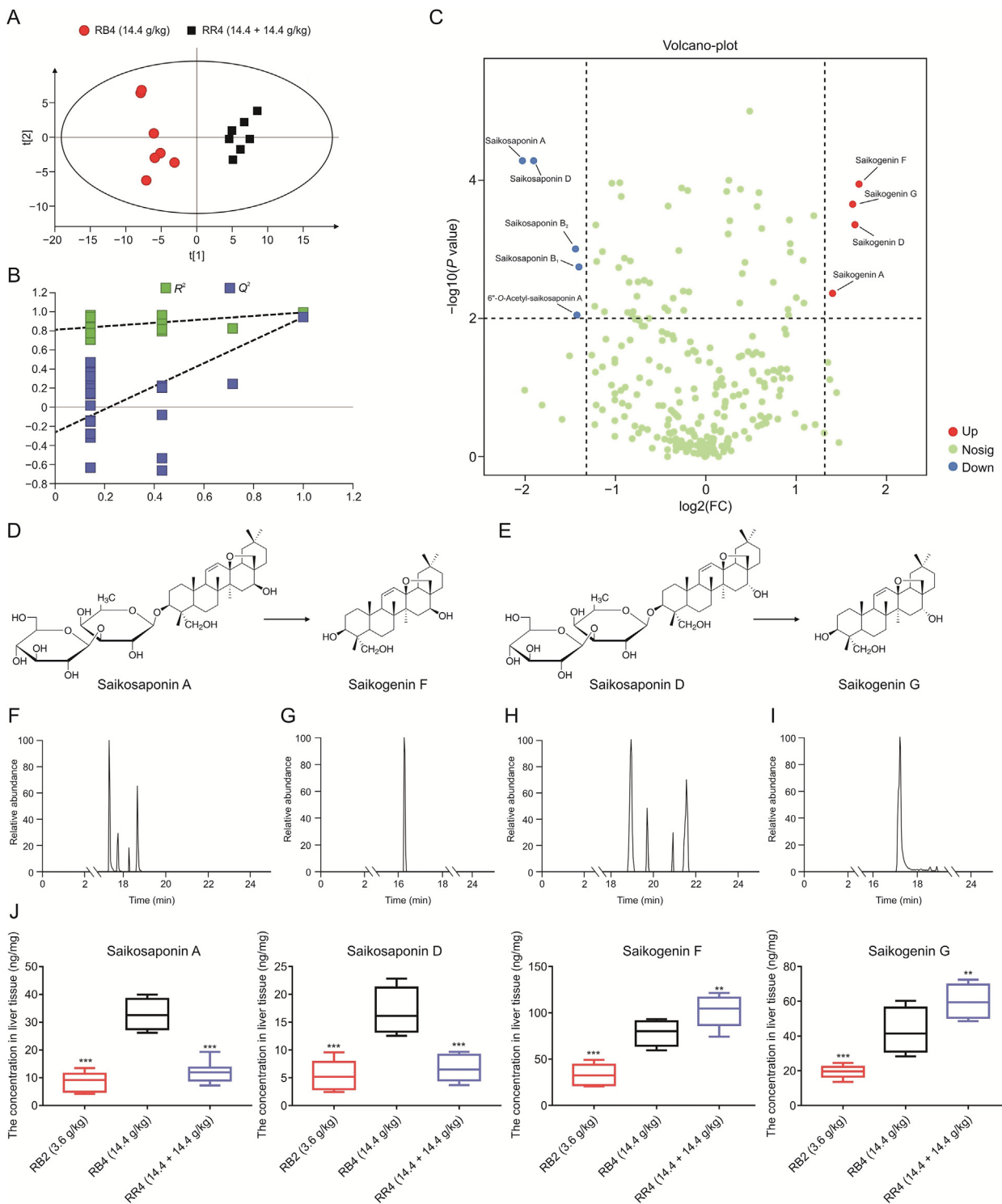
Fig. 5. The combined use of RPA and RB (RR group) promotes the conversion of saikosaponins to saikogenins in the liver compared with RB alone. (A) principal component analysis (PCA) score plots of liver chemical composition between RB alone (RB4 group) and in combination with RPA (RR4 group) ($n = 7$). (B) Orthogonal partial least squares-discriminant analysis (OPLS-DA) model validation diagram (the values of R^2X, R^2Y, and Q^2 were 0.445, 0.992, and 0.944, respectively). (C) Volcano plot showing the spread of 9 differentially altered components (5 components were significantly decreased and 4 components were significantly increased in the RR4 group compared to the RB4 group). (D) Chemical structure of saikosaponin A and saikogenin F. Solid arrows represent deglycosylation transitions. (E) Chemical structures of saikosaponin D and saikogenin G. Solid arrows represent deglycosylation transitions. (F) Typical parallel reaction monitoring (PRM) chromatograms of saikosaponin A, saikosaponin B₂, saikosaponin B₁, and saikosaponin D (17.314 min, 17.753 min, 18.244 min, and 18.674 min). (G) Typical PRM chromatograms of saikosaponin C (16.288 min). (H) Typical PRM chromatograms of saikogenin D, saikogenin A, and saikogenin G (18.951 min, 19.683 min, 20.916 min, and 21.608 min). (I) Typical PRM chromatograms of saikogenin E (17.199 min). (J) Concentration (ng/mg) of saikosaponin A, saikosaponin D, saikogenin F, and saikogenin G in the rat liver tissues. RB: Radix Bupleuri; RR: Radix Bupleuri-Radix Paeoniae Alba herb pair. Data are presented as the mean ± standard deviation (SD) ($n = 7$). P values were calculated using one-way analysis of variance (ANOVA) for multiple comparisons. **$P < 0.01$ and ***$P < 0.001$ compared with the RB4 group.
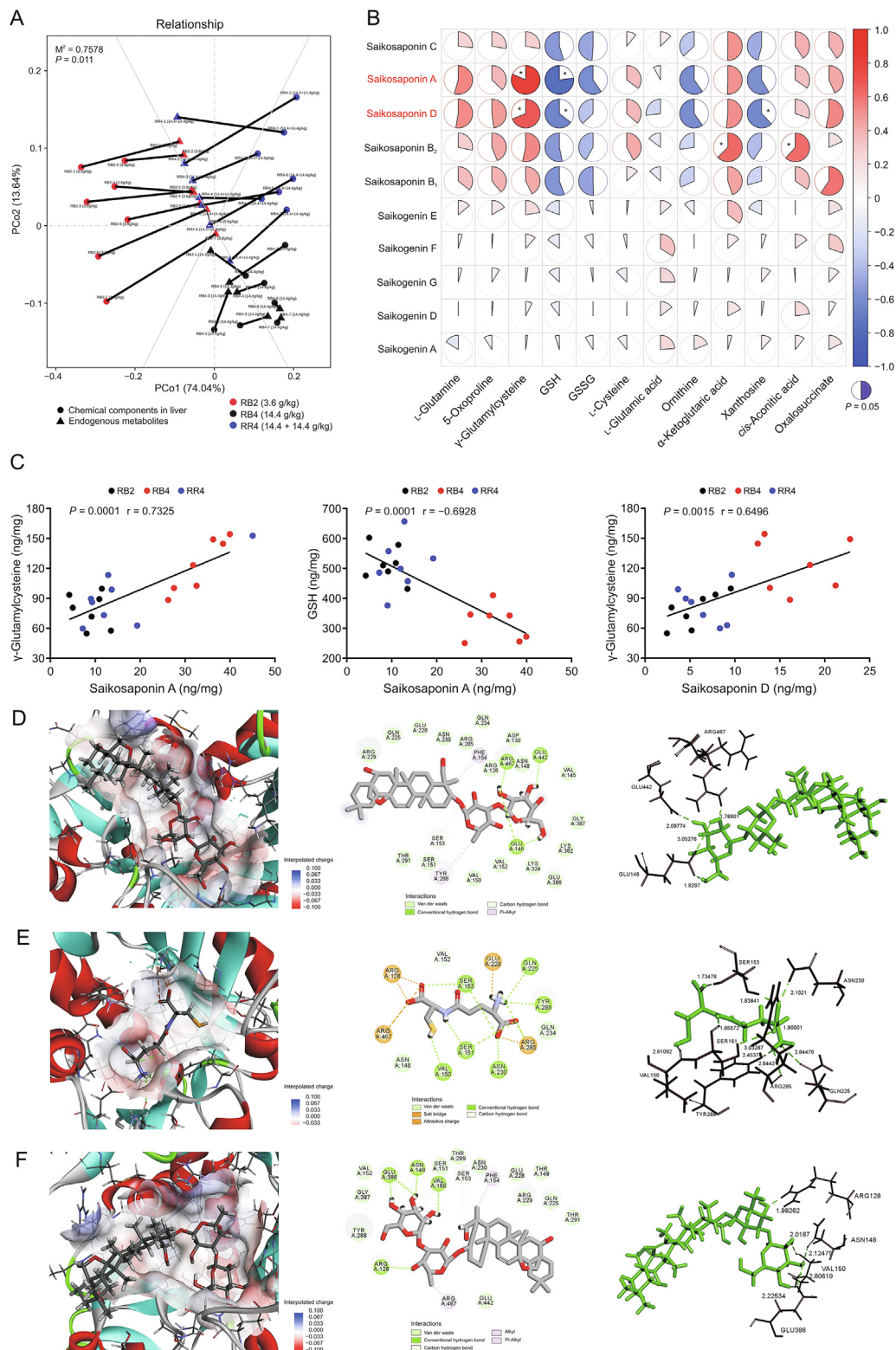
Fig. 6. Radix Paeoniae Alba (RPA)-suppressed RB-induced hepatotoxicity is associated with promoting the conversion of saikosaponins. (A) Procrustes analysis between the differential exogenous chemical components and the differential endogenous metabolites. (B) The heatmap of Pearson correlation analysis of the differential exogenous chemical components and the differential endogenous metabolites. Red indicates that r was a positive value, and blue indicates that r was a negative value. The darker the color, the larger the |r|. * means $P < 0.05$ and |r| > 0.6. (C) Scatter plot of the correlation analysis. (D) The detailed docking mode of GSS with saikosaponin A. (E) The detailed docking mode of GSS with its substrate (γ-glutamylcysteine). (F) The detailed docking mode of GSS with saikosaponin D. GSS: glutathione synthase; GSH: glutathione; GSSG: oxidized glutathione; RB: Radix Bupleuri; RR: Radix Bupleuri-Radix Paeoniae Alba herb pair.
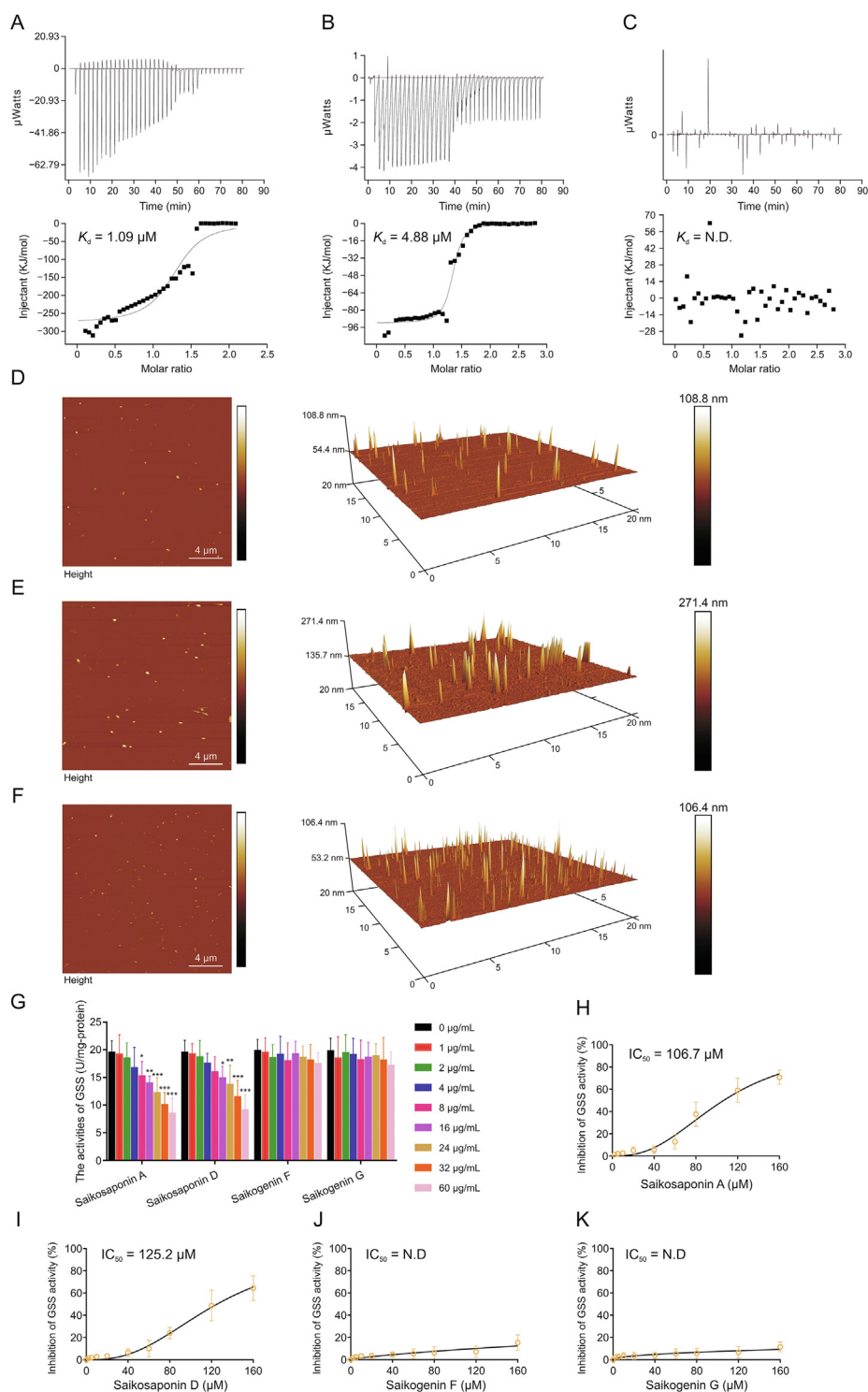
Fig. 7. Saikosaponin A and saikosaponin D have an inhibitory effect on GSS enzymes, while their deglycosylated conversion products saikogenin F and saikogenin G do not. (A–C) Isothermal titration calorimetry (ITC) experiments showed that saikosaponin A and saikosaponin D could directly combine with the GSS protein, but their deglycosylation conversion products saikogenin F and saikogenin G failed. The affinity activity of γ-glutamylcysteine-GSS (A), saikosaponin A-GSS (B), and saikogenin F-GSS (C) binding was analyzed by the ITC assay. (D–F) Atomic force microscopy (AFM) imaging technology was applied to further verify the interaction of the GSS protein with saikosaponin A and saikosaponin D. 2D and 3D microscopic images of GSS (D), GSS and saikosaponin A (E), GSS and saikogenin F (F). (G) The inhibitory activities of GSS were determined in an enzyme cocktail prepared from fresh rat liver homogenates. Data are presented as the mean ± standard deviation (SD) ($n = 6$). P values were calculated using one-way analysis of variance (ANOVA) for multiple comparisons. $^*P < 0.05$, $^{**}P < 0.01$, and $^{***}P < 0.001$ compared with 0 μg/mL. (H–K) IC$_{50}$ values of saikosaponin A, saikosaponin D, saikogenin F, and saikogenin G for the GSS protein. Recombinant GSS protein was used as the kinase, and γ-glutamylcysteine and glycine were used as substrates. The mixtures were incubated with saikosaponin A (H), saikosaponin D (I), saikogenin F (J), and saikogenin G (K) for 1 h at 37 °C for the GSS activity assay. The data shown are average values with SD of 3 experiments. K_d: kinetic constant; N.D.: not detected; GSS: glutathione synthetase; IC$_{50}$: half maximal inhibitory concentrations.
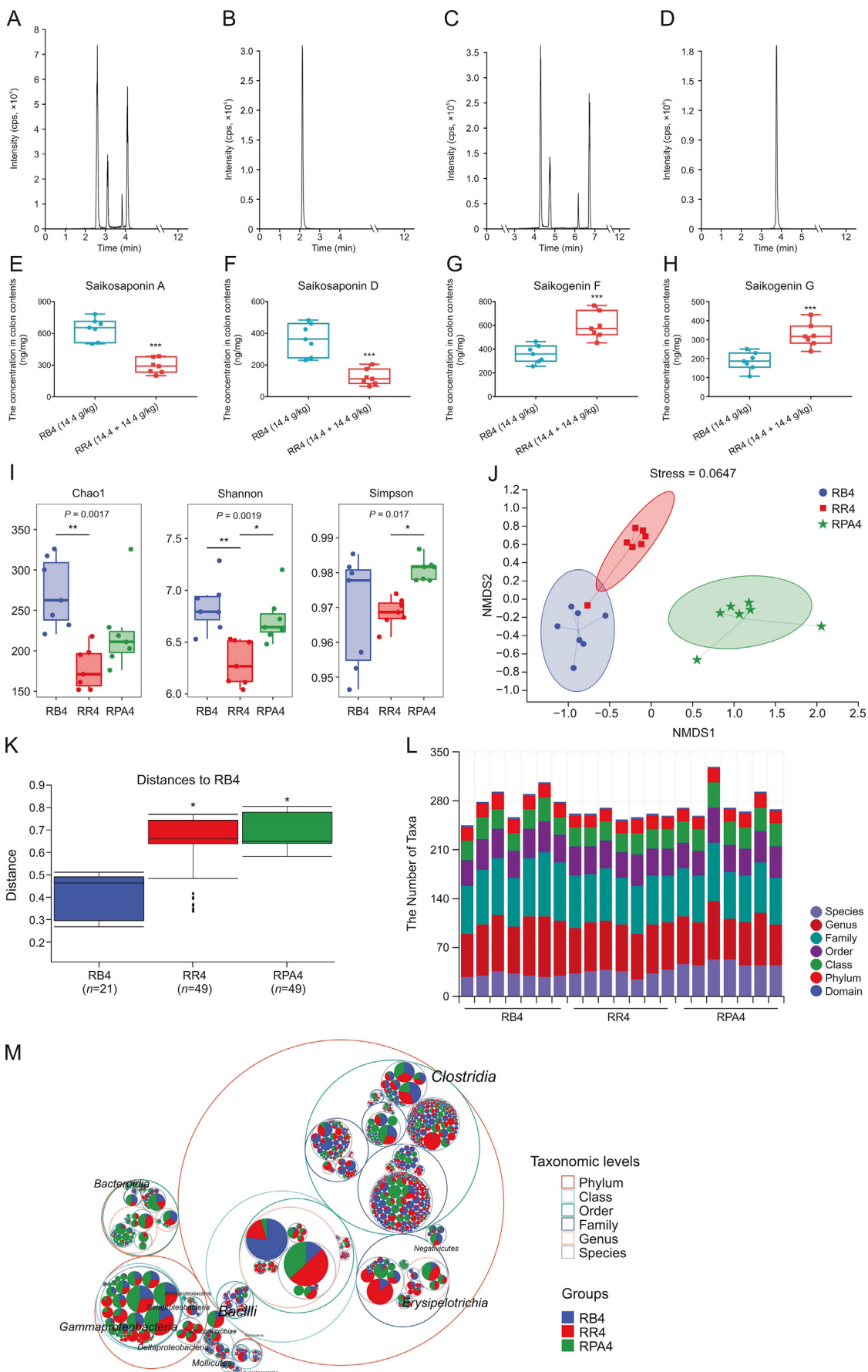
example, γ-glutamylcysteine was significantly negatively correlated with the tear secretion of STT ($r = -0.6498$, $P = 0.0105$) and significantly positively correlated with the water intake ($r = 0.6014$, $P = 0.0221$); GSH was significantly negatively correlated with AST and ALT ($r = -0.6715$, $P = 0.0096$; $r = -0.6112$, $P = 0.0201$, respectively, Fig. 2J). These results indicated that GSS may be a potential target of RB-induced hepatotoxicity.

3.4. RB4 inhibits GSS enzyme activity but does not regulate the protein level, which could be reversed by RPA treatment (RR4)

Following this lead, the targeted quantitative analysis of the glutathione metabolism pathway was performed by the MRM modes of UHPLC-Q-TRAP 3200/MS (Fig. S7). The compound-dependent parameters, including MRM ion pairs, CE, and DP are listed in Table S4. And the method validation results of the targeted quantitative analysis are shown in Tables S9−12. The results confirm that the analytical method was stable and reliable, and met the requirements for quantitative analysis of biological samples. In addition, the targeted quantitative analysis results confirmed that the substrate concentration (γ-glutamylcysteine) of GSS was significantly increased and that the product concentration (GSH) of GSS was significantly decreased in the RB4 group compared with the Control, CUMS, RB2, and RR4 groups (Fig. 3A), indicating that the activity of GSS was suppressed in the RB4 group. Next, the protein expression and activity of GSS were assayed whether GSS is a potential target of RPA to reverse RB-induced hepatotoxicity. This result showed that RB4 did not affect the protein level of GSS (Figs. 3B and C). However, RB4 significantly suppressed GSS activity compared with the Control, CUMS, and RB2 groups (Fig. 3D), suggesting that RB4 affected GSS functions mainly by modifying the four-dimensional structure of GSS protein and further inhibiting its activity. Meanwhile, RR4 significantly reversed the downregulation of GSS activity compared with that in the RB4 group (Fig. 3D). In summary, RB4 inhibits GSS enzyme activity but does not regulate the protein level, and RPA treatment (RR4) can reverse the inhibitory effect of RB4 on GSS enzymatic activity. These results indicate that GSS is a potential target of RPA to reverse RB-induced hepatotoxicity.

3.5. RPA suppresses RB-induced hepatotoxicity via oxidative stress and the NF-κB/NLRP3 pathway due to inhibition of GSS

GSH is a major antioxidant that is important for maintaining cellular redox balance and preventing oxidative injury. Studies have shown that the inhibition of GSS limits GSH synthesis, leading to the dysregulation of the GSH/GSSG ratio, thereby disrupting the redox balance in vivo, which in turn causes liver damage through activated oxidative stress and NF-κB inflammatory signaling pathways (Fig. 4A) [16−18,34]. Therefore, the GSH levels, GSH/GSSG ratio, MDA levels, SOD, and GSH-Px activities in the liver were determined. These results showed that the liver GSH level, GSH/GSSG ratio, SOD, and GSH-Px activities were significantly decreased, and the liver MDA levels were significantly increased in

the RB4 group compared with the Control, CUMS, and RB2 groups (Figs. 3A and 4B−F). Meanwhile, RB-induced liver GSH/GSSG ratio dysregulation and oxidative stress activation were significantly reversed after combined administration with RPA (RR4 group) (Figs. 4B−F). Previous studies have demonstrated that oxidative stress promotes liver inflammation by activating the NF-κB/NLRP3 signaling pathway [16,35]. Thus, the NF-κB/NLRP3 pathway was analyzed to determine whether it was related to RPA-suppressing RB-induced hepatotoxicity. Western blotting demonstrated that RB4 significantly elevated the ratio of phosphorylated NF-κB p65 to total NF-κB p65 (p-NF-κB p65/NF-κB p65) (Figs. 4G and H), indicating that the NF-κB/NLRP3 signaling pathway was activated in RB-induced hepatotoxicity. However, RPA treatment (RR4 group) downregulated the ratio of p-p65/p65 (Figs. 4G and H), indicating that RPA suppressed RB-induced activation of the NF-κB signaling pathway. Furthermore, the protein expression of NLRP3, caspase-1, and ASC was significantly elevated in the RB4 group, which could also be reversed by RPA treatment (RR4) (Figs. 4I−K). In addition, ELISA results showed that RB-induced IL-1β, IL-6, and TNF-α production in the liver was significantly inhibited after combined administration with RPA (RR4 group) (Figs. 4L−N). Taken together, RPA suppressed RB-induced hepatotoxicity via oxidative stress and the NF-κB/NLRP3 inflammatory pathway.

3.6. RPA-suppressed RB-induced hepatotoxicity is associated with promoting the conversion of saikosaponins to saikogenins in the liver

Our previous studies showed that the combined use of RB and RPA could promote the conversion of saikosaponins to saikogenins in serum compared with RB alone [27]. Moreover, the hepatotoxicity of saikosaponins has also been reported in many studies [9,22,23]. Therefore, we speculated that RPA-suppressed RB-induced hepatotoxicity was related to promoting the metabolic transformation of saikosaponins in the liver. First, the difference in liver chemical composition between RB alone (RB4 group) and RB combined with RPA (RR4 group) was analyzed by integrating background subtraction, similarity analysis techniques, and multivariate statistical analysis techniques. The details of background subtraction [36,37] and similarity analysis techniques [38,39] are provided in Supplemental Method 7 and Supplemental Method 12, respectively. A total of 287 exogenous MS data points from RB were obtained through the background subtraction algorithm and similarity analysis techniques (Fig. S8). Then, the 287 exogenous MS data from RB were further imported into SIMCA-P 16.0 (Umetrics, Sweden) for multivariate statistical analysis. The PCA score plots showed that the RB4 group was separated from the RR4 group (Figs. 5A and B). Furthermore, the differential chemical composition between RB4 and RR4 were screened according to the −log10 $P > 2$ and log2 Ratio (4RB/4RR) < -1.2 or >1.2. The results indicated that the separated profile consisted of 9 significantly altered components, with 5 components (saikosaponin A, saikosaponin D, saikosaponin B_2, saikosaponin B_1, 6″-O-acetyl-saikosaponin A) being significantly decreased and 4 components (saikogenin F, saikogenin

Fig. 8. RPA promotes the conversion of saikosaponins to saikogenins in vivo and is related to the regulation of intestinal microflora composition. (A) Typical multiple reaction monitoring (MRM) chromatograms of saikosaponin A, saikosaponin B_2, saikosaponin B_1, and saikosaponin D (2.58 min, 3.11 min, 3.82 min, and 4.08 min). (B) Typical MRM chromatograms of saikosaponin C (2.12 min). (C) Typical MRM chromatograms of saikogenin F, saikogenin D, saikogenin A, and saikogenin G (4.28 min, 4.73 min, 6.17 min, and 6.71 min). (D) Typical MRM chromatograms of saikogenin E (3.76 min). (E−H) Concentration (ng/mg) of saikosaponin A (E), saikosaponin D (F), saikogenin F (G), and saikogenin G (H) in colon contents. (I) Alpha diversity analysis of gut bacterial richness (Chao1 index) and diversity (Shannon index and Simpson index) from different groups ($n = 7$). (J) Beta diversity index of Bray−Curtis-based nonmetric multidimensional scaling (NMDS) analysis from different groups ($n = 7$). (K) Permutational multivariate analysis of variance (PERMANOVA) of Bray−Curtis-based NMDS (permutations = 999), $^*P < 0.01$ compared with the RB4 group. (L) The number of taxa at the domain, phylum, class, order, family, genus, and species levels by taxonomic annotation of species. (M) Taxonomic tree in packed circles. Taxonomic differences are based on 16S rRNA gene sequences extracted from the metagenome. The largest circles represent the phylum level, and the inner circles represent class, family, genus, and species. RB: Radix Bupleuri; RPA: Radix Paeoniae Alba; RR: Radix Bupleuri-Radix Paeoniae Alba herb pair. All data are expressed as the mean ± standard deviation (SD) ($n = 7$). P values were calculated using two-tailed Student's t-test for paired comparisons or one-way analysis of variance (ANOVA) for multiple comparisons. $^*P < 0.05$, $^{**}P < 0.01$ and, $^{***}P < 0.001$ compared with the RB4 group.

A

The current LDA threshold is 3.5

RB4
RR4

a: p__Cyanobacteria
b: p__Firmicutes
c: p__Proteobacteria
d: p__Tenericutes
e: p__Verrucomicrobia
f: c__Mollicutes
g: c__Clostridia
h: c__Erysipelotrichia
i: c__Negativicutes
j: c__Deltaproteobacteria
k: c__Gammaproteobacteria
l: c__Verrucomicrobiae
m: o__Bacillales
n: o__Clostridiales
o: o__Erysipelotrichales
p: o__Acidaminococcales
q: o__Desulfovibrionales
r: o__Enterobacterales
s: o__Verrucomicrobiales
t: f__Paenibacillaceae
u: f__Peptostreptococcaceae
v: f__Bacteroidaceae
w: f__Enterococcaceae
x: f__Clostridiaceae
y: f__Lachnospiraceae
z: f__Ruminococcaceae
a1: f__Erysipelotrichaceae

b1: f__Acidaminococcaceae
c1: f__Desulfovibrionaceae
d1: f__Enterobacteriaceae
e1: f__Akkermansiaceae
f1: g__Prevotella
g1: g__Enterococcus
h1: g__Butyricicoccus
i1: g__Clostridium
j1: g__Ihubacter
k1: g__Blautia
l1: g__Ruminococcus
m1: g__Erysipelatoclostridium
n1: g__Desulfovibrio
o1: g__Bacteroides
p1: g__Phascolarctobacterium
q1: g__Escherichia
r1: g__Akkermansia
s1: s__Bacteroides_fragilis
t1: s__Bacteroides_vulgatus
u1: s__Lactobacillus_intestinalis
v1: s__Lactobacillus_koreensis
w1: s__Lactobacillus_murinus
x1: s__Lactobacillus_reuteri
y1: s__Phascolarctobacterium_faecium
z1: s__Escherichia_coli
a2: s__Akkermansia_muciniphila

B

The current LDA threshold is 3.5

RB4
RR4

C

D

g_Bacteroides

E

s-Escherichia_coli

F

s-Lactobacillus_koreensis

G, saikogenin D, and saikogenin A) being significantly increased in the RR4 group compared to the RB4 group (Fig. 5C). These results indicated that the combined use of RB and RPA promotes the conversion of saikosaponins to saikogenins in the liver compared with RB alone (Figs. 5D and E). The detailed identification data of the differential components are provided in Table S13.

To further confirm that the combined use of RB and RPA can promote the metabolic transformation of saikosaponins in the liver, quantitative analysis of the saikosaponins (saikosaponin A, saikosaponin D, saikosaponin B_2, saikosaponin B_1, and saikosaponin C) and saikogenins (saikogenin E, saikogenin F, saikogenin G, saikogenin D, and saikogenin A) was performed by PRM mode of UPLC-Q-Orbitrap/MS. The optimized normalized collision energy (NCE) and the quantitative ion are shown in Table S2, the typical PRM chromatograms of the saikosaponins and saikogenins are shown in Figs. 5F–I, and the method validation results of the targeted quantitative analysis are shown in Tables S14–17. The quantitative analysis results confirmed that saikosaponin A, saikosaponin D, saikosaponin B_2, and saikosaponin B_1 were significantly decreased and that saikogenin F, saikogenin G, saikogenin D, and saikogenin A were significantly increased in the RR4 group compared to the RB4 group (Figs. 5J and S9), indicating that the combined use of RB and RPA could promote the conversion of saikosaponins to saikogenins in the liver compared to RB alone.

Furthermore, based on the investigation of chemical component profiles and endogenous metabolite profiles, correlation analysis was used to find the potential link between significantly altered chemical components and regulated endogenous metabolites between the RB4 group and RR4 group. First, Procrustes analysis results showed that there was a good correlation between the differential exogenous chemical components and the differential endogenous metabolites (Fig. 6A, $M^2 = 0.7578$, $P = 0.011$). Next, Pearson correlation analysis further confirmed that there was a significant correlation between the substrates and products of GSS and saikosaponins (Fig. 6B). As illustrated in Figs. 6C and S7, saikosaponin A and saikosaponin D were significantly positively correlated with γ-glutamylcysteine, which was a substrate of the GSS enzyme ($r = 0.7325$, $P = 0.0001$; $r = 0.6496$, $P = 0.0015$, respectively, Fig. 6C). In addition, saikosaponin A and saikosaponin D were significantly negatively correlated with GSH, which is a product of the GSS enzyme ($r = -0.6928$, $P = 0.0001$; $r = -0.6176$, $P = 0.0029$, respectively, Figs. 6C and S10). These results indicated that saikosaponin A and saikosaponin D have potential inhibitory effects on GSS enzymes. Therefore, we speculated that RPA alleviates the inhibitory effect on GSS enzymes by promoting the conversion of saikosaponins, thereby suppressing RB-induced hepatotoxicity.

3.7. Saikosaponin A and saikosaponin D have a competitive inhibitory effect on GSS, but their deglycosylation conversion products saikogenin F and saikogenin G do not

The above results show that RB inhibits GSS enzyme activity rather than the protein level. Furthermore, the results also indicated that saikosaponin A and saikosaponin D in RB had potential inhibitory effects on enzymes. Therefore, we speculated that saikosaponin A and saikosaponin D may affect GSS functions mainly by regulating its activity. Next, we employed molecular docking and

isothermal titration calorimetry (ITC) assays to explore the molecular mechanism of GSS protein inhibition. γ-glutamylcysteine, an endogenous substrate for GSS enzymes, was chosen as the positive control. In silico molecular docking analysis demonstrated that saikosaponin A and saikosaponin D fit comfortably into the binding pocket of γ-glutamylcysteine with similar binding positions, and they showed similar docking performance when docked with GSS enzymes, with binding free energies of −9.80 kcal/mol for saikosaponin A, −9.37 kcal/mol for saikosaponin D, and −11.02 kcal/mol for γ-glutamylcysteine (Figs. 6D–F). However, as deglycosylation conversion products, saikogenin F and saikogenin G failed to dock with the catalytic site of GSS in silico, suggesting that the glycoside was presumably necessary for binding to GSS.

The kinetic constant (K_d) was used as an assessment for the affinity of the compound−protein interaction. Subsequently, the K_d values between GSS and saikosaponin A, saikosaponin D, γ-glutamylcysteine, saikogenin F, and saikogenin G were further verified by the ITC test. As expected, the results suggested that saikosaponin A and saikosaponin D presented similar GSS protein affinities compared with γ-glutamylcysteine, with K_d values for saikosaponin A-GSS and saikosaponin D-GSS of 4.88 μM and 5.81 μM, respectively, close to the value of γ-glutamylcysteine-GSS of 1.09 μM (Figs. 7A, 7B and S11A). However, their deglycosylation conversion products saikogenin F and saikogenin G exhibited no binding activity (Figs. 7C and S11B). In addition, the number of binding sites for saikosaponin A-GSS, saikosaponin D-GSS, and γ-glutamylcysteine-GSS was 1.21 ± 0.01, 0.99 ± 0.02, and 1.46 ± 0.03, respectively. This result confirmed that there was only one binding site between GSS and saikosaponin A, saikosaponin D, and γ-glutamylcysteine. Meanwhile, the ΔH values for saikosaponin A-GSS, saikosaponin D-GSS, and γ-glutamylcysteine-GSS were $(-0.92 \pm 0.02) \times 10^5$ J/mol, $(-1.06 \pm 0.03) \times 10^5$ J/mol, and $(-2.76 \pm 0.09) \times 10^5$ J/mol, respectively; the ΔS values for saikosaponin A-GSS, saikosaponin D-GSS, and γ-glutamylcysteine-GSS were −181 J/mol/deg, −227 J/mol/deg, and −791 J/mol/deg, respectively (Table S18). These results confirm that the binding of GSS with saikosaponin A, saikosaponin D, and γ-glutamylcysteine is mainly hydrogen bonding and van der Waals forces. Furthermore, the atomic force microscopy (AFM) imaging technique was applied to further verify the interaction of the GSS protein with saikosaponin A and saikosaponin D. As shown in Figs. 7D–F, 3D microscopic imaging revealed that the average height of free GSS was 68.6 ± 40.1 nm (Fig. 7D). When the GSS protein interacts with saikosaponin A and saikosaponin D, the GSS protein adsorbed on the quartz sheet expands violently, with average heights of 151.3 ± 53.1 nm and 106.7 ± 65.7 nm, respectively (Figs. 7E and S12A). However, when incubated with saikogenin F and saikogenin G, there was no significant change in the height of the GSS protein (Figs. 7F and S12B). These results showed that saikosaponin A and saikosaponin D were directly combined with the GSS protein, while saikogenin F and saikogenin G could not. The same results were confirmed by the in vitro GSS inhibitory activity assay (Figs. 7G−K). The results showed that saikosaponin A and saikosaponin D could significantly suppress the activity of GSS in a dose-dependent manner (Fig. 7G), with half maximal inhibitory concentrations (IC_{50}) of 106.7 μM and 125.2 μM, respectively (Fig. 7H and I). Meanwhile, saikogenin F and saikogenin G had no significant effect

Fig. 9. Full-length 16S rRNA sequencing shows altered microbiota composition among the RB4, RR4, and RPA4 groups. (A, B) Taxonomic cladogram (A) and LDA histogram (B) obtained from LEfSe analysis showed the significantly enriched microbiome between the RB4 and RR4 groups ($P < 0.05$ and LDA >3.5). (C) Heatmap of significantly altered bacteria in the colon contents of the RB4, RR4, and RPA4 groups. Bacteria with LDA >3.5 of LEfSe analysis and $P < 0.05$ were considered to be significantly different. (D–F) The relative abundance of *Bacteroides* (D), *Escherichia_coli* (E), and *Lactobacillus_koreensis* (F) among the RB4, RR4, and RPA4 groups. LDA: linear discriminant analysis; RB: Radix Bupleuri; RPA: Radix Paeoniae Alba; RR: Radix Bupleuri-Radix Paeoniae Alba herb pair. All data are expressed as the mean ± standard deviation (SD) ($n = 7$). P values were calculated using one-way analysis of variance (ANOVA) for multiple comparisons. $^*P < 0.05$, $^{**}P < 0.01$, and $^{***}P < 0.001$ compared with the RB4 group.
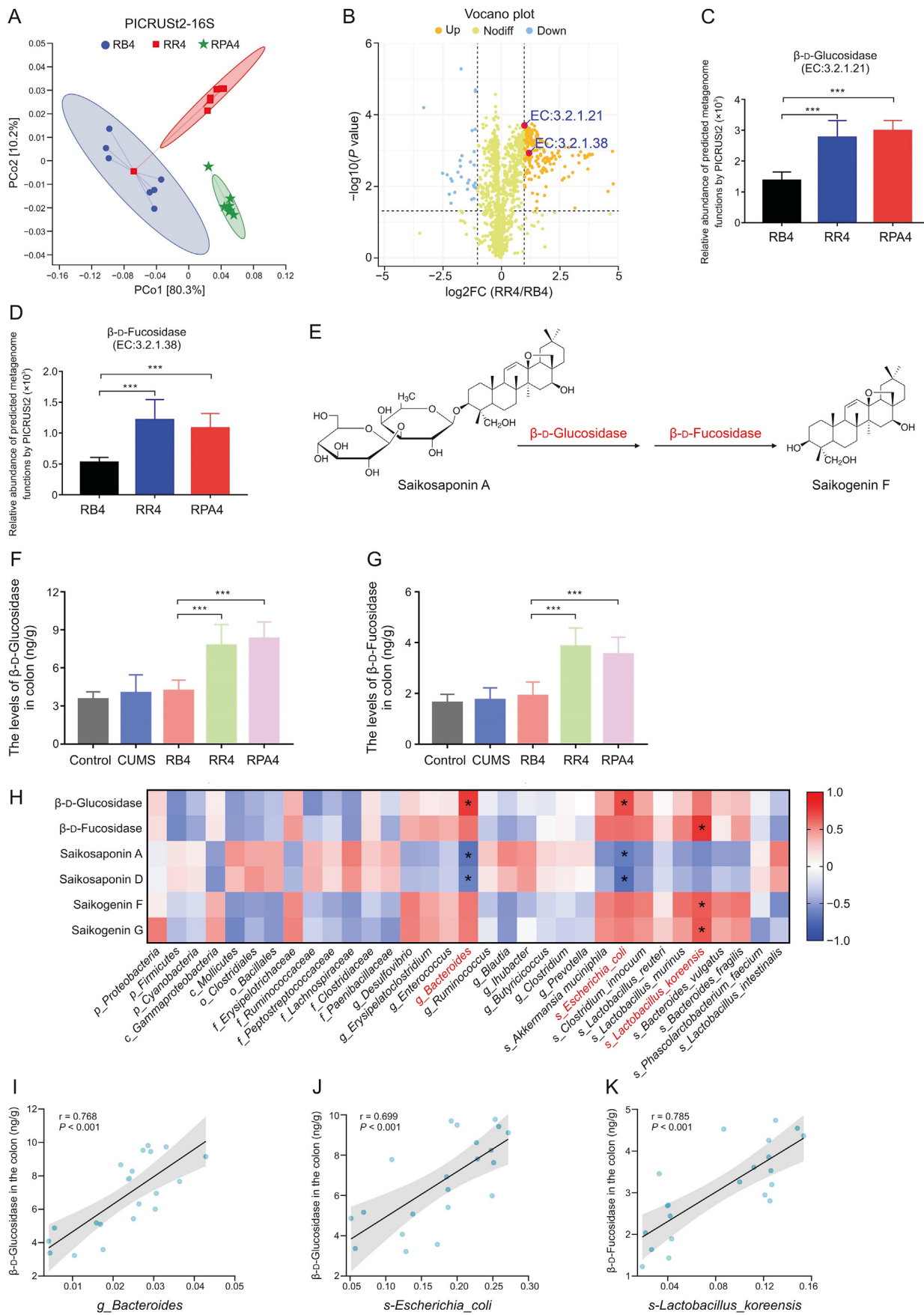
on the activity of GSS (Fig. 7J and K). In conclusion, the ITC analyses, AFM imaging analyses, and in vitro GSS inhibitory activity experiment indicated that saikosaponin A and saikosaponin D exhibit relatively strong binding with GSS protein and inhibit GSS enzyme activity at the present concentrations, while their deglycosylated conversion products saikogenin F and saikogenin G do not.

3.8. RPA altered gut microbiota composition and increased Bacteroides, Escherichia_coli, and Lactobacillus_koreensis levels, leading to the promotion of the conversion of saikosaponins to saikogenins in vivo

As one of the main sites of drug metabolism, the intestine has important effects on drug absorption, metabolism, bioactivity, and toxicity [40]. It has been reported in the literature that saikosaponins are mainly transformed into the corresponding saikogenins by intestinal microflora with glycosidase activity [24,25]. Moreover, the quantitative analysis of saikosaponins and saikogenins in colon contents revealed that the main site of RPA-promoted conversion of saikosaponins to saikogenins occurs in the intestine (Figs. 8A–H and S13, and Tables S19–22). Therefore, we speculated that RPA may promote the conversion of saikosaponins to saikogenins in vivo by regulating intestinal microflora. To test this speculation, we utilized 16S rRNA third-generation full-length sequencing to determine whether RPA promotion of the conversion of saikosaponins to saikogenins in vivo was related to the regulation of intestinal microflora composition. The evaluation of full-length 16S rRNA sequencing data of the intestinal microflora is presented in Fig. S14. Alpha (Fig. 8I) and beta (Figs. 8J and K) diversity analyses showed that there were significant differences among the RB4, RR4, and RPA4 groups. In addition, full-length 16S rRNA sequencing revealed the composition of the gut microbiome in each group. The results showed that there were significant differences in the composition and abundance of the gut microbiome among the RB4, RR4, and RPA4 groups (Figs. 8L, 8M, and S15).

To identify the different bacteria between the RB4 and RR4 groups, we performed LEfSe analysis based on the linear discriminant analysis (LDA) score >3.5 and $P < 0.05$ (Figs. 9A and B). In total, 33 significantly different bacteria were screened between the RB4 and RR4 groups (Fig. 9C). Among them, 23 different bacteria had the same significant regulatory trend between the RR4 and RPA4 groups compared with the RB4 group (Fig. 9C). Notably, at the genus level, the relative abundance of *Bacteroides* increased significantly in the RR4 and RPA4 groups compared to the RB4 group (Fig. 9D). And at the species level, the relative abundance of *Escherichia_coli* and *Lactobacillus_koreensis* increased significantly in the RR4 and RPA4 groups compared to the RB4 group (Figs. 9E and F).

Next, bacterial functions were predicted via phylogenetic investigation of communities by reconstruction of unobserved states 2 (PICRUSt2) based on 16S marker sequences, as previously reported [41]. The principal coordinate analysis (PCoA) plot of the prediction of metagenome functional profiles depicted that the bacterial functional profiles among the RB4, RR4, and RPA4 groups were separated (Fig. 10A). Furthermore, the differential bacterial

functions between RB4 and RR4 were screened according to -log10 $P > 1.3$ and Log2FC (RR4/RB4) < −1 or >1. The results indicated that the relative abundances of β-D-glucosidase and β-D-fucosidase were significantly increased in the RR4 group compared to the RB4 group (Figs. 10B–D). Notably, β-D-glucosidase and β-D-fucosidase were the two key enzymes involved in converting saikosaponins into saikogenins (Fig. 10E). Following this lead, the levels of β-D-glucosidase and β-D-fucosidase in the colon tissues were tested. Consistently, the results also showed that the levels of β-D-glucosidase and β-D-fucosidase in the colon tissues were significantly increased in the RR4 and RPA4 groups compared to the RB4 group (Figs. 10F and G). These results indicated that RPA increases the abundance of intestinal bacteria with β-D-glucosidase and β-D-fucosidase activity in the intestine, thereby promoting the conversion of saikosaponins to saikogenins.

Based on the evidence above, we next determined the relationship between the significantly altered gut microbiota and β-D-glucosidase, β-D-fucosidase, saikosaponin A, saikosaponin D, saikogenin F, and saikogenin G in the colon using correlation analysis. Correlation analysis results demonstrated that *Bacteroides* and *Escherichia_coli* were significantly negatively correlated with saikosaponin A and saikosaponin D and significantly positively correlated with β-D-glucosidase, respectively (Figs. 10H–J, and S16A–D). Meanwhile, *Lactobacillus_koreensis* was significantly positively correlated with β-D-fucosidase, saikogenin F, and saikogenin G (Figs. 10K, and S16E and S16F). Notably, it has been previously documented that *Bacteroides* and *Escherichia_coli* have β-D-glucosidase activity, which can deglycosylate ginsenosides [42–44]. Moreover, *Lactobacillus_koreensis* has β-D-glucosidase and β-D-fucosidase activity, which can convert saikosaponins to saikogenins [45]. This result suggested that *Bacteroides*, *Escherichia_coli*, and *Lactobacillus_koreensis* play a pivotal role in facilitating the conversion of saikosaponins to saikogenins. In addition, the relative abundance of *Bacteroides*, *Escherichia_coli* and *Lactobacillus_koreensis* increased significantly in the RR4 and RPA4 groups compared to the RB4 group (Figs. 9D–F). These results indicated that RPA promoted the conversion of saikosaponins to saikogenins in the colon by increasing the abundance of *Bacteroides*, *Escherichia_coli*, and *Lactobacillus_koreensis*.

4. Conclusion

In this work, our study aims to investigate the mechanisms by which RPA attenuates RB-induced hepatotoxicity. The results showed that RPA increased the abundance of intestinal bacteria with glycosidase activity in the intestine, thereby promoting the conversion of saikosaponins to saikogenins. Different from saikosaponin A and saikosaponin D, which are directly combined with GSS as an inhibitor, their deglycosylation conversion products saikogenin F and saikogenin G exhibited no GSS binding activity. Based on this, RPA can effectively alleviate the inhibitory effect of saikosaponins on GSS activity and reshape the liver redox balance by increasing the GSH-GSSG ratio. Meanwhile, RPA inhibited RB-induced liver oxidative injury and alleviated the liver inflammatory response mediated by the NF-κB/NLRP3 pathway. In

Fig. 10. RPA promotes the conversion of saikosaponins to saikogenins in vivo by increasing the levels of *Bacteroides*, *Escherichia_coli*, and *Lactobacillus_koreensis*. (A) Principal coordinate analysis (PCoA) plot of the prediction of metagenome functions from 16S marker sequences by PICRUSt2 among the RB4, RR4, and RPA4 groups ($n = 7$). (B) Volcano plot of significantly altered bacterial functions predicted by PICRUSt2 between the RB4 and RR4 groups. Bacterial functions with Log2FC (RR4/RB4) > 1 or < −1 and −log10 $P > 1.3$ were considered to be significantly different. (C) Relative abundance of β-D-glucosidase predicted by PICRUSt2 using 16S amplicons. (D) Relative abundance of β-D-fucosidase predicted by PICRUSt2 using 16S amplicons. (E) Saikosaponin A was converted to saikogenin F via intestinal bacteria with β-D-glucosidase and β-D-fucosidase activity. (F) The levels of β-D-glucosidase in the colon. (G) The levels of β-D-fucosidase in the colon. (H) Spearman correlation analysis of the significantly altered gut microbiota and β-D-glucosidase, β-D-fucosidase, saikosaponin A, saikosaponin D, saikogenin F, and saikogenin G in the colon. Red indicates that r was a positive value, and blue indicates that r was a negative value. The darker the color, the larger the |r|. * means $P < 0.05$ and |r| > 0.6. (I–K) Scatter plot of the correlation analysis. PICRUSt2: phylogenetic investigation of communities by reconstruction of unobserved states 2; PCo: principal coordinate; RB: Radix Bupleuri; RPA: Radix Paeoniae Alba; RR: Radix Bupleuri-Radix Paeoniae Alba herb pair. All data are expressed as the mean ± standard deviation (SD) ($n = 7$). P values were calculated using one-way analysis of variance (ANOVA) for multiple comparisons. ***$P < 0.001$ compared with the RB4 group.

conclusion, the present study suggests that promoting the conversion of saikosaponins by modulating gut microbiota composition to attenuate the inhibitory effect on GSS activity is a potential mechanism by which RPA prevents RB-induced hepatotoxicity.

CRediT author statement

Congcong Chen: Methodology, Validation, Formal analysis, Investigation, Data curation, Writing - Original draft preparation, Visualization; Wenxia Gong: Methodology, Validation, Formal analysis, Investigation, Data curation; Junshen Tian and Xiaoxia Gao: Conceptualization, Methodology, Writing - Reviewing and Editing; Xuemei Qin, Guanhua Du, and Yuzhi Zhou: Resources, Writing - Reviewing and Editing, Supervision, Funding acquisition.

Declaration of competing interest

The authors declare that there are no conflicts of interest.

Acknowledgments

Appendix A. Supplementary data

Supplementary data to this article can be found online at https://doi.org/10.1016/j.jpha.2023.04.016.

References

[1] I.A. Khan, T. Smillie, Implementing a "quality by design" approach to assure the safety and integrity of botanical dietary supplements, J. Nat. Prod. 75 (2012) 1665–1673.

[2] P. Zhang, Y.G. Ye, X.Z. Yang, et al., Systematic review on Chinese herbal medicine induced liver injury, Evid. Based Complement. Alternat. Med. 2016 (2016), 3560812.

[3] T. Shen, Y.X. Liu, J. Shang, et al., Incidence and etiology of drug-induced liver injury in mainland China, Gastroenterology 156 (2019) 2230–2241.e11.

[4] F.D. Yang, X.X. Dong, X.B. Yin, et al., Radix *bupleuri*: A review of traditional uses, botany, phytochemistry, pharmacology, and toxicology, Biomed. Res. Int. 2017 (2017), 7597596.

[5] P. Wang, X.X. Gao, M.L. Liang, et al., Dose-effect/toxicity of bupleuri *Radix* on chronic unpredictable mild stress and normal rats based on liver metabolomics, Front. Pharmacol. 12 (2021), 627451.

[6] D.C.H. Teo, P.S.L. Ng, S.H. Tan, et al., Drug-induced liver injury associated with complementary and alternative medicine: A review of adverse event reports in an Asian community from 2009 to 2014, BMC. Complement. Altern. Med. 16 (2016), 192.

[7] X.X. Gao, M.L. Liang, Y. Fang, et al., Deciphering the differential effective and toxic responses of bupleuri *Radix* following the induction of chronic unpredictable mild stress and in healthy rats based on serum metabolic profiles, Front. Pharmacol. 8 (2018), 995.

[8] H. Jiang, L. Yang, A.J. Hou, et al., Botany, traditional uses, phytochemistry, analytical methods, processing, pharmacology and pharmacokinetics of Bupleuri *Radix*: A systematic review, Biomed. Pharmacother. 131 (2020), 110679.

[9] X.J.Y. Li, X.Y. Li, N.N. Huang, et al., A comprehensive review and perspectives on pharmacology and toxicology of saikosaponins, Phytomedicine 50 (2018) 73–87.

[10] X. Li, X.M. Qin, J.S. Tian, et al., Integrated network pharmacology and metabolomics to dissect the combination mechanisms of *Bupleurum chinense DC-Paeonia lactiflora Pall* herb pair for treating depression, J. Ethnopharmacol. 264 (2021), 113281.

[11] Y. Jin, Z.L. Huang, L. Li, et al., Quercetin attenuates toosendanin-induced hepatotoxicity through inducing the Nrf2/GCL/GSH antioxidant signaling pathway, Acta Pharmacol. Sin. 40 (2019) 75–85.

[12] Q.N. Liang, Y.C. Sheng, P. Jiang, et al., The gender-dependent difference of liver GSH antioxidant system in mice and its influence on isoline-induced liver injury, Toxicology 280 (2011) 61–69.

[13] S.C. Lu, Regulation of glutathione synthesis, Mol. Aspects Med. 30 (2009) 42–59.

[14] L.D. DeLeve, N. Kaplowitz, Glutathione metabolism and its role in hepatotoxicity, Pharmacol. Ther. 52 (1991) 287–305.

[15] J.L. Luo, F. Hammarqvist, K. Andersson, et al., Surgical trauma decreases glutathione synthetic capacity in human skeletal muscle tissue, Am. J. Physiol. Endocrinol. Metab. 275 (1998) E359–E365.

[16] L.Y. Yuan, N. Kaplowitz, Glutathione in liver diseases and hepatotoxicity, Mol. Aspects Med. 30 (2009) 29–41.

[17] S.C. Lu, Glutathione synthesis, Biochim. Biophys. Acta BBA Gen. Subj. 1830 (2013) 3143–3153.

[18] P. Chen, L. Wang, S.T. Sun, et al., High-throughput screening suggests glutathione synthetase as an anti-tumor target of polydatin using human proteome chip, Int. J. Biol. Macromol. 161 (2020) 1230–1239.

[19] R.K. Weersma, A. Zhernakova, J. Fu, Interaction between drugs and the gut microbiome, Gut 69 (2020) 1510–1519.

[20] Y.H. Li, Q. Meng, M.B. Yang, et al., Current trends in drug metabolism and pharmacokinetics, Acta Pharm. Sin. B 9 (2019) 1113–1144.

[21] H. Kida, T. Akao, M.R. Meselhy, et al., Enzymes responsible for the metabolism of saikosaponins from *Eubacterium* sp. A-44, a human intestinal anaerobe, Biol. Pharm. Bull. 20 (1997) 1274–1278.

[22] X.Y. Li, X.J.Y. Li, J.X. Lu, et al., Saikosaponins induced hepatotoxicity in mice via lipid metabolism dysregulation and oxidative stress: A proteomic study, BMC Complement. Altern. Med. 17 (2017), 219.

[23] Q.Q. Zhang, W.Q. Huang, Y.Q. Gao, et al., Metabolomics reveals the efficacy of caspase inhibition for saikosaponin D-induced hepatotoxicity, Front. Pharmacol. 9 (2018), 732.

[24] J.J. Liu, Y.W. Xue, J.B. Sun, et al., Pharmacokinetics and oral bioavailability studies of three saikogenins in rats using a validated UFLC-MS/MS method, J. Chromatogr. B Analyt. Technol. Biomed. Life Sci. 1124 (2019) 265–272.

[25] Q.W. Liu, Y.W. Xue, J.J. Liu, et al., Saikosaponins and the deglycosylated metabolites exert liver meridian guiding effect through PXR/CYP3A4 inhibition, J. Ethnopharmacol. 279 (2021), 114344.

[26] S.Q. Ren, J.J. Liu, Y.W. Xue, et al., Comparative permeability of three saikosaponins and corresponding saikogenins in Caco-2 model by a validated UHPLC-MS/MS method, J. Pharm. Anal. 11 (2021) 435–443.

[27] C.C. Chen, J.S. Tian, X.X. Gao, et al., An integrated strategy to study the combination mechanisms of *Bupleurum chinense* DC and *Paeonia lactiflora Pall* for treating depression based on correlation analysis between serum chemical components profiles and endogenous metabolites profiles, J. Ethnopharmacol. 305 (2023), 116068.

[28] X. Chen, Z. Yang, Y. Xu, et al., Progress and prediction of multicomponent quantification in complex systems with practical LC-UV methods, J. Pharm. Anal. 13 (2023) 142–155.

[29] C.C. Chen, Q.C. Yin, J.S. Tian, et al., Studies on the potential link between antidepressant effect of Xiaoyao San and its pharmacological activity of hepatoprotection based on multi-platform metabolomics, J. Ethnopharmacol. 249 (2020), 112432.

[30] S.T. Yu, J.X. Fan, L. Zhang, et al., Assessment of biphasic extraction methods of mouse fecal metabolites for liquid chromatography-mass spectrometry-based metabolomic studies, J. Proteome Res. 20 (2021) 4487–4494.

[31] Y.R. Zhu, F. Wang, J.T. Han, et al., Untargeted and targeted mass spectrometry reveal the effects of theanine on the central and peripheral metabolomics of chronic unpredictable mild stress-induced depression in juvenile rats, J. Pharm. Anal. 13 (2023) 73–87.

[32] R.J. Andrade, G.P. Aithal, E.S. Björnsson, et al., EASL clinical practice guidelines: Drug-induced liver injury, J. Hepatol. 70 (2019) 1222–1261.

[33] Z.Q. Li, Q.Q. Fan, M.L. Chen, et al., The interaction between polyphyllin I and SQLE protein induces hepatotoxicity through SREBP-2/HMGCR/SQLE/LSS pathway, J. Pharm. Anal. 13 (2023) 39–54.

[34] C. Zhang, N. Wang, Y. Xu, et al., Molecular mechanisms involved in oxidative stress-associated liver injury induced by Chinese herbal medicine: An experimental evidence-based literature review and network pharmacology study, Int. J. Mol. Sci. 19 (2018), 2745.

[35] H. Li, L. Yuan, X.Y. Li, et al., Isoorientin attenuated the pyroptotic hepatocyte damage induced by benzo[a]pyrene via ROS/NF-κB/NLRP3/caspase-1 signaling pathway, Antioxidants (Basel) 10 (2021), 1275.

[36] H.Y. Zhang, M. Grubb, W. Wu, et al., Algorithm for thorough background subtraction of high-resolution LC/MS data: Application to obtain clean product ion spectra from nonselective collision-induced dissociation experiments, Anal. Chem. 81 (2009) 2695–2700.

[37] G.L. Yan, A.H. Zhang, H. Sun, et al., An effective method for determining the ingredients of Shuanghuanglian formula in blood samples using high-resolution LC-MS coupled with background subtraction and a multiple data processing approach, J. Sep. Sci. 36 (2013) 3191–3199.

[38] G.X. Xie, S.L. Wang, H. Zhang, et al., Poly-pharmacokinetic study of a multicomponent herbal medicine in healthy Chinese volunteers, Clin. Pharmacol. Ther. 103 (2018) 692–702.

[39] G.X. Xie, A.H. Zhao, L.L. Zhao, et al., Metabolic fate of tea polyphenols in humans, J. Proteome Res. 11 (2012) 3449–3457.

[40] R.K. Weersma, A. Zhernakova, J.Y. Fu, Interaction between drugs and the gut microbiome, Gut 69 (2020) 1510–1519.

[41] G.M. Douglas, V.J. Maffei, J.R. Zaneveld, et al., PICRUSt2 for prediction of metagenome functions, Nat. Biotechnol. 38 (2020) 685–688.

[42] R.F. Thornton, E.C. Murphy, T.F. Kagawa, et al., The effect of environmental conditions on expression of *Bacteroides fragilis* and *Bacteroides thetaiotaomicron* C10 protease genes, BMC Microbiol. 12 (2012), 190.

[43] E.A. Bae, M.J. Han, E.J. Kim, et al., Transformation of ginseng saponins to ginsenoside Rh$_2$ by acids and human intestinal bacteria and biological activities of their transformants, Arch. Pharm. Res. 27 (2004) 61–67.

[44] I. Tryland, L. Fiksdal, Enzyme characteristics of β-D-galactosidase- and β-D-glucuronidase-positive bacteria and their interference in rapid methods for detection of waterborne coliforms and *Escherichia coli*, Appl. Environ. Microbiol. 64 (1998) 1018–1023.

[45] J.E. Lee, B.K. Song, J.H. Kim, et al., Production of prosaikogenin F, prosaikogenin G, saikogenin F and saikogenin G by the recombinant enzymatic hydrolysis of saikosaponin and their anti-cancer effect, Molecules 27 (2022), 3255.